

MULTIRESOLUTION-BASED MESH ADAPTATION AND ERROR CONTROL FOR LATTICE BOLTZMANN METHODS WITH APPLICATIONS TO HYPERBOLIC CONSERVATION LAWS

THOMAS BELLOTTI*, LOÏC GOUARIN*, BENJAMIN GRAILLE†, AND MARC MASSOT*

Abstract. Lattice Boltzmann Methods (LBM) stand out for their simplicity and computational efficiency while offering the possibility of simulating complex phenomena. While they are optimal for Cartesian meshes, adapted meshes have traditionally been a stumbling block since it is difficult to predict the right physics through various levels of meshes. In this work, we design a class of fully adaptive LBM methods with dynamic mesh adaptation and error control relying on multiresolution analysis. This wavelet-based approach allows to adapt the mesh based on the regularity of the solution and leads to a very efficient compression of the solution without loosing its quality and with the preservation of the properties of the original LBM method on the finest grid. This yields a general approach for a large spectrum of schemes and allows precise error bounds, without the need for deep modifications on the reference scheme. An error analysis is proposed. For the purpose of assessing the approach, we conduct a series of test-cases for various schemes and scalar and systems of conservation laws, where solutions with shocks are to be found and local mesh adaptation is especially relevant. Theoretical estimates are retrieved while a reduced memory footprint is observed. It paves the way to an implementation in a multi-dimensional framework and high computational efficiency of the method for both parabolic and hyperbolic equations, which is the subject of a companion paper.

Key words. Lattice Boltzmann Method, multiresolution analysis, wavelets, dynamic mesh adaptation, error control, hyperbolic conservation laws

AMS subject classifications. 76M28 65M50 42C40 65M12 35L65

1. Introduction. A wide class of systems representing various complex phenomena across different disciplines (fluid mechanics, combustion, atmospheric sciences, plasma physics or biomedical engineering, see [22, 13, 17] and references therein for a few examples) are modeled through PDEs, the solution of which can involve dynamically moving fronts, usually very localized in space. Among these PDEs, one can find the fluid dynamics Euler equations, and more generally hyperbolic systems of conservation laws, where shock wave solutions are to be found. For such solutions, we need a good level of spatial detail where steep variations occur, whereas one can accept a coarse space discretization where large *plateaux* are present. An effective way of reducing the overall cost of a numerical solvers consists in devising a strategy to dynamically adapt the spatial discretization to the solution as time advances, aiming at performing less operations and limiting the memory footprint, while preserving a proper resolution. Once a discretization in space is chosen, several strategies exist to conduct mesh adaptation, ranging from patch-based and cell-based Adaptive Mesh Refinement (AMR) to multiresolution (MR) techniques. Such strategies can make a crucial difference in terms of time-to-solution and allow scientists to strongly reduce computational cost or reach the solution of large 3D problems on standard machines.

The discretization of the original PDEs can be conducted relying on several methods: here we focus on Lattice Boltzmann schemes (LBM - Lattice Boltzmann Methods), a class of wide-spread numerical methods to approximate models which can have spatially non-homogeneous solutions. Despite being present in the community since the end of the eighties, they have gained a lot of attention in the last decade due to the evolution of the computer architectures and body of literature on their mathematical

*CMAP, CNRS, Ecole polytechnique, Institut Polytechnique de Paris, 91128 Palaiseau Cedex, France. thomas.bellotti@polytechnique.edu

†Institut de Mathématiques d’Orsay, Université Paris-Saclay, 91405 Orsay Cedex, France.

analysis. Mesh-adaptation for LBM has been a stumbling block for quite some time even if interesting pieces of solution have been provided. The key issue is related to the difficulty of predicting the right physics through various levels of meshes. This can also lead to delicate transmission conditions for acoustic waves and has been a relatively hot topic in the field.

The purpose of the present contribution is to design of a new numerical strategy for LBM with dynamic mesh adaptation and error control based on multiresolution analysis. The key issue is the ability to rely on the original LBM scheme on the finest mesh without alteration while still reaching a controlled level of accuracy on the compressed representation. This contribution focuses on setting the fundamentals of the method, we concentrate on the one-dimensional framework and provide an error analysis. We conduct a numerical assessment on various test-cases for hyperbolic conservation laws (scalar and systems). We have chosen such a framework since it is a very representative example of localized fronts with lack of regularity, where the MR can play a key role and where we can test a large variety of LBM schemes. The method yields a very reduced memory footprint while preserving a given level of accuracy. The proposed numerical strategy is versatile and can be extended in a straightforward manner to parabolic and hyperbolic systems in multi-dimensions, which is out of the scope of the present paper but is the subject of a companion contribution [1]. Before entering the body of the contribution, let us describe the state of the art.

1.1. Lattice Boltzmann methods and mesh adaptation. The lattice Boltzmann methods are relatively recent computational techniques for the numerical solution of PDEs, introduced at the end of the eighties by McNamara and Zanetti [41] and by Higuera and Jimenez [33], and stemming from the “Lattice gas automata”. The derivation of the method starts from Boltzmann equation, with a simplified collision kernel¹, and relies on the selection of a small set of discrete velocities compatible with a given fixed-step lattice. This strategy is widely employed in many areas of computational mathematics, with special mention to the Computational Fluid Dynamics (CFD). In this context, the method has been used to simulate the Navier-Stokes system at low Mach numbers [38] with more recent extensions to handle multi-phase problems ([36] for a review), along with systems of hyperbolic conservation laws [29]. The advantages of the method are its dramatic simplicity² and the ease of parallelization. Still, stability, consistency and convergence remain open topics.

To the best of our knowledge, LBM strategies on adapted grids have been only developed either on fixed grids, in the spirit of Filippova and Hänel [26] and of many subsequent works, where more refined patches are placed according to an *a priori* knowledge of the flow. Such fixed refinement zones also yield difficulties in aeroacoustics resolution related to the artificial transmission impedance of the refinement interface [28, 25, 34]. Another strategy is to use an AMR approach [2] with some heuristics to determine the need for refinement in certain areas. In this class, we find the work of Fakhari and Lee [24] using the magnitude of the vorticity and its derivatives as regularity indicator, while Eitel-Amor *et al.* [23] have employed a weighted vorticity and the energy difference with respect to a free flow solution. Crouse *et al.* [11] have used the weighted magnitude of the divergence of the velocity field. Finally, Wu and Shu [48] have considered the difference between solutions at successive time

¹Through the BGK approximation with single or multiple relaxation times.

²Since overall the strategy decomposes into a local collision and a stream along the characteristics of the discrete velocities

steps. Although these approaches have been certainly able to reduce the computational cost of the simulations, they still face several drawbacks which we summarize as follows:

- Few available methods are time-adaptive: most of the time, one must construct a fixed non-uniform mesh according to some *a priori* knowledge of the solution. The refinement interface can then induce spurious effects on the numerical simulations when fine-scale physics interfere with a coarse level of the mesh. An example of such a situation is the resolution of acoustic waves leading to purely numerical transmission defaults. Consequently, this approach is intrinsically problem-dependent and non-optimal for unsteady solutions.
- Most of the time the reference scheme has to be deeply manipulated at various levels of grid to preserve the macroscopic parameters of the system.
- One must devise a heuristic, the dynamic mesh adaptation will rely on. As a consequence, there is no control on the compression error.

In this work, we propose a strategy to fill these gaps by introducing a time adaptive numerical approach, designed to work for any LBM scheme without need for manipulations, which grants a precise bound on the compression error.

1.2. Multiresolution analysis. Multiresolution analysis has proved to be a general tool to analyze the local regularity of a signal in a rigorous setting, based on its decomposition on a wavelet basis. It has been introduced in the seminal works by Daubechies [12], Mallat [40] and Cohen *et al.* [7]. The possibility of applying this mechanism to reduce the computational cost of a numerical method was studied a few years later by Harten [31, 32, 3] in the context of Finite Volumes methods for conservation laws. The principle was to use multiresolution to reduce the number of computations to evaluate fluxes at the interfaces, claiming that they constitute the majority of the computational cost. However, this approach still computes the solution on the full uniform mesh. The possibilities offered by multiresolution had been further exploited by Cohen *et al.* [8] who, in the footsteps of Harten, have developed fully adaptive schemes with solutions updated only on the reduced grid. Thus, multiresolution is not only a way of computing a large number of fluxes more cheaply, but also a manner to compute fewer of them. Both these strategies grant better time-performances than traditional approaches on uniform grids in addition to a precise control on the additional error, unlike most of the AMR techniques. This strategy has been lately used to tackle various kinds of problems with Finite Volumes methods. We mention parabolic conservation laws by Roussel *et al.* [45], the compressible Navier-Stokes equations in Bramkamp *et al.* [4], the shallow water equations by Lamby *et al.* [39], multi-component flows by Coquel *et al.* [10], degenerate parabolic equations by Burger *et al.* [5] and finally the Euler system with a local time-stepping technique again by Coquel *et al.* [9]. Furthermore, this technique has been included in later works to address more complex problems, such as flames [44, 18, 13] or by coupling it with other numerical strategies: we mention the works of Duarte *et al.* [19, 22, 17] and N’Guessan *et al.* [43]. We are not aware of the use of such procedure to conduct mesh adaptation and error control on LBM schemes. We decided to adopt a volumetric vision for MR because since it is naturally conservative, even if a whole body of literature exists about point-wise multiresolution [30, 6, 27].

1.3. Paper organization. We present the formalism of LBM schemes and Multiresolution analysis in section 2 and 3; the fundamentals of the proposed numerical strategy and theoretical error analysis is presented in section 4. Section 5 is dedicated to numerical verifications on scalar and hyperbolic systems of conservation laws with

a variety of LBM schemes, before concluding in section 6.

2. Lattice Boltzmann schemes. Consider a uni-dimensional bounded domain $\Omega = [a, b]$ with $a < b$ and the maximum level of allowed refinement $\bar{J} \in \mathbb{N}$. The domain is discretized by a partition of $2^{\bar{J}}$ with measure $\Delta x_{\bar{J}} = 2^{-\bar{J}}(b-a)$ forming a collection $\mathcal{L}_{\bar{J}} := (I_{\bar{J},k})_{k=0,\dots,2^{\bar{J}}-1}$ called lattice. Once we consider a function $f(t, x)$ of time and space, we define – in a Finite Volumes fashion – its spatial averages on each cell

$$F_k(t) = \frac{1}{|I_{\bar{J},k}|} \int_{I_{\bar{J},k}} f(t, x) dx, \quad t \geq 0, \quad k = 0, \dots, 2^{\bar{J}} - 1.$$

Henceforth, every discretized quantity shall be interpreted as a mean value of an underlying integrable function over the cell it refers to. In all the work, we consider a finite temporal horizon $t \in [0, T]$ with $T > 0$. The time is discretized, as we shall see in a moment, in equally spaced time steps with step $\Delta t > 0$. Without loss of generality, we assume that T has been chosen so that $N := T/\Delta t \in \mathbb{N}$. Thus we indicate $t^n := n\Delta t$ for $n = 0, \dots, N$ and $F_k^n \simeq F_k(t^n)$ for $k = 0, \dots, 2^{\bar{J}} - 1$ and $n = 0, \dots, N$. From now on $\|\cdot\|_{\ell^p}$ shall denote the weighted ℓ^p norm for $p \in [1, \infty]$ over $\mathbb{R}^{2^{\bar{J}}}$ with weight $\Delta x_{\bar{J}}$.

2.1. The d’Humières formalism. We consider lattice Boltzmann schemes under the so-called d’Humières formalism [15]. Let $\lambda > 0$ be a lattice velocity, so that the time step Δt can be defined using the acoustic scaling³ $\Delta t = \Delta x_{\bar{J}}/\lambda$. Moreover, consider a set of discrete velocities $\{v^h\}_{h=0,\dots,q-1}$, where $q \in \mathbb{N}$, compatible with the lattice velocity λ in the sense that $w^h := v^h/\lambda \in \mathbb{Z}$ for $h = 0, \dots, q-1$. At time t^n , we indicate with $F_k^{h,n}$ the density of the population moving with velocity v^h at the cell $k = 0, \dots, 2^{\bar{J}} - 1$ for every $h = 0, \dots, q-1$. In order to recover the so-called moments, we consider an invertible matrix $\mathbf{M} \in \mathbb{R}^{q \times q}$ defining the change of variables to pass from the space of the population densities towards the space of moments by $(M^0, \dots, M^{q-1})^T = \mathbf{M}(F^0, \dots, F^{q-1})$, where we do not indicate the space at the time coordinates because the change of basis is completely local.

The lattice Boltzmann scheme can be divided into two phases: collision phase and stream phase. We indicate its action as

$$(F_k^{h,n+1})_{\substack{k=0,\dots,2^{\bar{J}}-1 \\ h=0,\dots,q-1}} = \mathbf{L}(F_k^{h,n})_{\substack{k=0,\dots,2^{\bar{J}}-1 \\ h=0,\dots,q-1}},$$

for any $n = 0, \dots, N-1$. The operator \mathbf{L} is constructed as follows.

2.1.1. Collision phase. Let us consider a cell $k = 0, \dots, 2^{\bar{J}} - 1$, then the collision phase is a local linear relaxation of the non-conserved moments towards their equilibrium, namely

$$\begin{aligned} M_k^{h,n^*} &= M_k^{h,n}, & h = 0, \dots, q_{\text{cons}} - 1, \\ M_k^{h,n^*} &= (1 - s^h)M_k^{h,n} + s^h M^{h,\text{eq}}(M_k^{0,n}, \dots, M_k^{q_{\text{cons}}-1,n}), & h = q_{\text{cons}}, \dots, q-1, \end{aligned}$$

where $q_{\text{cons}} < q$ is the number of conserved moments and where s^h and $M^{h,\text{eq}}$ are respectively the relaxation parameter and the equilibrium of the h^{th} moment, which is a non-linear function of the conserved moments. These quantities are set relying either on a Chapman-Enskog expansion or on the theory of equivalent equations introduced by Dubois [20] in order to be consistent with the equations we want to solve.

³Still, the strategy of this work equally works for a parabolic scaling such as $\Delta t \sim (\Delta x_{\bar{J}})^2$ [1].

2.1.2. Stream phase. Again on a cell $k = 0, \dots, 2^{\bar{J}} - 1$, the stream phase is given by

$$F_k^{h,n+1} = F_{k-w^h}^{h,n*}, \quad h = 0, \dots, q-1.$$

As we shall be interested in considering all the populations together, in the sequel, the weighted ℓ^p norm are extended from $\mathbb{R}^{2^{\bar{J}}}$ to $\mathbb{R}^{q2^{\bar{J}}}$ in the usual way.

3. Adaptive multiresolution. Following the approach by [8, 16], the starting point of the multiresolution analysis is to consider a hierarchy of $L+1$ with $L \in \mathbb{N}$ nested uni-variate lattices \mathcal{L}_j with $j = \bar{J} - L, \dots, \bar{J}$, given by

$$\mathcal{L}_j := (I_{j,k})_{k=0, \dots, N_j-1}, \quad \text{with } I_{j,k} := [(b-a)2^{-j}k + a, (b-a)2^{-j}(k+1) + a],$$

for $j = \underline{J}, \dots, \bar{J}$, where we have set $\underline{J} := \bar{J} - L$ and $N_j := 2^j$ for $j = \underline{J}, \dots, \bar{J}$. They form a sequence of progressively finer nested lattices as we observe that each cell $I_{j,k}$ (called “father”) includes its two “children” $I_{j+1,2k}$ and $I_{j+1,2k+1}$ (called “brothers”) rendering a tree-like structure. As done before, given a function $f(t, x)$, we have to understand things in the following way

$$f_{j,k}^n \approx \frac{1}{|I_{j,k}|} \int_{I_{j,k}} f(t^n, x) dx,$$

for $n = 0, \dots, N$, $j = \underline{J}, \dots, \bar{J}$ and $k = 0, \dots, N_j - 1$. In the remaining part of this Section, since time is of no importance, we do not mention the dependence of any quantity on it for the sake of clarity.

3.1. Projection and prediction operator. The projection and the prediction operators allow one to navigate in the ladder of nested lattices up and down. We start from the projection operator, which takes information at a certain level of resolution $j+1$ and transforms it into information on a coarser level j as illustrated in Figure 1.

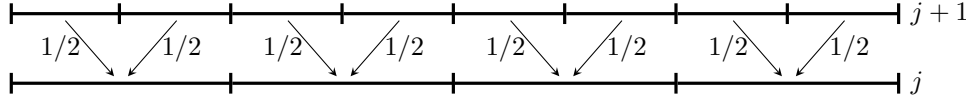


FIG. 1. Illustration of the action of the projection operator. The cell average on the cell at level j is reconstructed by taking the average of the values on its two children at level $j+1$.

DEFINITION 3.1 (Projection operator). *The projection operator $\mathbf{P}_\vee : \mathbb{R}^2 \rightarrow \mathbb{R}$ is defined by*

$$f_{j,k}^h = \mathbf{P}_\vee \left((f_{j+1,2k+\delta}^h)_{\delta=0,1} \right) = \frac{1}{2} (f_{j+1,2k}^h + f_{j+1,2k+1}^h),$$

for every $h = 0, \dots, q-1$, $j = \underline{J}, \dots, \bar{J}$ and $k = 0, \dots, N_j - 1$.

The opposite happens for the prediction operator (Figure 2), taking information on a certain level j and trying to recover an estimation of the values on a finer level $j+1$. It seems that we have an infinity of possible choices and this is indeed the case. However, we impose, following Cohen *et al.* [8], some reasonable rigidity on the choice of the operator.

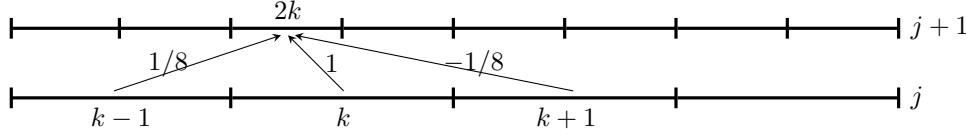


FIG. 2. Illustration of the action of the prediction operator taking $\gamma = 1$. The cell average on the cell at level $j+1$ is reconstructed by taking the values j of the father and his two neighbors with suitable weights.

DEFINITION 3.2 (Prediction operator). The prediction operator $\mathbf{P}_\wedge : \mathbb{R}^{1+w} \rightarrow \mathbb{R}^2$, giving approximated values (denoted by a hat) of means at a fine level from data on a coarse level, that is

$$\left(\widehat{f}_{j+1,2k+\delta}^h \right)_{\delta=0,1} = \mathbf{P}_\wedge \left((f_{j,\pi})_{\pi \in R(j,k)} \right),$$

for $h = 0, \dots, q-1$, $j = \underline{J}, \dots, \overline{J}-1$ and $k = 0, \dots, N_j-1$, where

- The operator is local, namely the outcome depends on the value on $1+w$ cells at level j with indices belonging to $R(j,k)$ geometrically close to $I_{j+1,2k+\delta}$ with $\delta = 0, 1$.
- The operator is consistent with the projection operator, namely

$$\mathbf{P}_\vee \left(\left(\widehat{f}_{j+1,2k+\delta}^h \right)_{\delta=0,1} \right) = f_{j,k}^h,$$

for $h = 0, \dots, q-1$, $j = \underline{J}, \dots, \overline{J}-1$ and $k = 0, \dots, N_j-1$.

REMARK 1 (Consequences of the definition). By the previous definition the father belongs to the prediction stencil of its sons (this is the 1 in the $1+w$). Also observe that this definition does not impose to consider linear operators, even if it is the choice for this and many preceding works [31, 32, 8, 16, 43, 42].

In particular, let $\gamma \in \mathbb{N}$ and consider for any $h = 0, \dots, q-1$, $j = \underline{J}, \dots, \overline{J}-1$ and $k = 0, \dots, N_j-1$

$$\widehat{f}_{j+1,2k+\delta}^h = f_{j,k}^h + (-1)^\delta \sum_{\alpha=1}^{\gamma} c_\alpha (f_{j,k+\alpha}^h - f_{j,k-\alpha}^h), \quad \delta = 0, 1,$$

corresponding to the polynomial centered interpolations, which are exact for the averages of polynomials up to degree 2γ , being accurate at order $\mu := 2\gamma + 1$. Some coefficients are given by (see [16, 47, 42] and references therein):

- $\gamma = 1$, with $c_1 = -1/8$.
- $\gamma = 2$, with $c_1 = -22/128$ and $c_2 = 3/128$.
- $\gamma = 3$, with $c_1 = -201/1024$, $c_2 = 11/256$ and $c_3 = 5/1024$.

3.2. Details and smoothness estimation. Intuitively, the more the predicted value is far from the actual value on the considered cell, the more we can assume that the function locally lacks in smoothness due to the fact that it is far from behaving polynomially. This is what is quantified by the notion of detail:

DEFINITION 3.3 (Detail). The details are defined as

$$d_{j,k}^h := f_{j,k}^h - \widehat{f}_{j,k}^h,$$

for $h = 0, \dots, q-1$, $j = \underline{J}+1, \dots, \bar{J}$.

The details are redundant between brothers $I_{j+1,2k}$ and $I_{j+1,2k+1}$ sharing the same father $I_{j,k}$. This is a trivial consequence of the consistency of \mathbf{P}_\wedge and reads

$$(3.1) \quad d_{j+1,2k}^h = -d_{j+1,2k+1}^h,$$

for $h = 0, \dots, q-1$, $j = \underline{J}, \dots, \bar{J}-1$ and $k = 0, \dots, N_{j-1}-1$. For this reason, we have to avoid the redundancy by considering only one detail between two brothers: we chose to keep only the one of the son with even indices $d_{j+1,2k}^h$ ⁴. Thus we introduce the sets of indices

$$\begin{aligned} \nabla_{\underline{J}} &:= \{(\underline{J}, k) \quad : \quad k = 0, \dots, N_{\underline{J}}-1\}, \\ \nabla_j &:= \{(j, k) \quad : \quad k = 0, \dots, N_j-1 \text{ and } k \text{ even}\}, \quad j = \underline{J}+1, \dots, \bar{J}. \end{aligned}$$

Hence we have constructed the multiresolution $\mathcal{M}_{\mathcal{R}}$ transform acting as follows

$$(3.2) \quad \mathbf{f}_{\underline{J}}^h \quad \begin{array}{c} \xrightarrow{\mathcal{M}_{\mathcal{R}}} \\ \xleftarrow{\mathcal{M}_{\mathcal{R}}^{-1}} \end{array} \quad (\mathbf{f}_{\underline{J}}^h, \mathbf{d}_{\underline{J}+1}^h, \dots, \mathbf{d}_{\bar{J}}^h),$$

for every $h = 0, \dots, q-1$, where

$$\begin{aligned} \mathbf{f}_j^h &:= (f_{j,k}^h)_{k=0, \dots, N_j-1}, \quad j = \underline{J}, \dots, \bar{J}, \\ \mathbf{d}_j^h &:= (d_{j,k}^h)_{(j,k) \in \nabla_j}, \quad j = \underline{J}+1, \dots, \bar{J}. \end{aligned}$$

One easily checks that each side of (3.2) contains the same number of elements, because we have eliminated the redundancy of the details. The details are a regularity indicator of the encoded function, as stated by the following Proposition

PROPOSITION 3.4 (Details decay). *Consider a cell $I_{j,k}$ for $j = \underline{J}+1, \dots, \bar{J}$ and a population $h = 0, \dots, q-1$ assuming that $f^h \in W_\infty^\nu(\tilde{\Sigma}_{j,k})$ for some $\nu \geq 0$, where $\tilde{\Sigma}_{j,k}$ is the support of the dual wavelet (see [16]) generated by the prediction operator \mathbf{P}_\wedge over the cell $I_{j,k}$ and*

$$W_p^\nu(I) := \{\phi \quad : \quad \phi^{(\eta)} \in L^p(I), \quad 0 \leq \eta \leq \nu\}, \quad \|\phi\|_{W_p^\nu(I)} := \|\phi\|_{L^p(I)} + |\phi|_{W_p^\nu(I)},$$

where the semi-norm is $|\phi|_{W_p^\nu(I)} := \|\phi^{(\nu)}\|_{L^p(I)}$. Then, we have the following decay estimate for the details

$$(3.3) \quad |d_{j,k}^h| \lesssim 2^{-j \min(\nu, \mu)} |f^h|_{W_\infty^{\min(\nu, \mu)}(\tilde{\Sigma}_{j,k})}.$$

Proof. Consider $\min(\nu, \mu) = \mu$ without loss of generality. Having adopted a volumetric approach, the L^1 normalization is the natural one for the dual wavelet. Thus, the conjugate exponent is $p = \infty$. Since $f^h \in W_\infty^\mu(\tilde{\Sigma}_{j,k})$, De Vore and Sharpley [14] show that there exists a polynomial $\bar{\pi} \in \Pi_{\mu-1}$ such that $\|f^h - \bar{\pi}\|_{L^\infty(\tilde{\Sigma}_{j,k})} \lesssim |\tilde{\Sigma}_{j,k}|^\mu |f^h|_{W_\infty^\mu(\tilde{\Sigma}_{j,k})}$, where the constant depends only on μ . Using the cancellation

⁴The opposite is perfectly fine.

property of the dual wavelet, the Hölder inequality, the normalization, the previous inequality and the fact that $|\tilde{\Sigma}_{j,k}| \lesssim 2^{-j}$

$$\begin{aligned} |d_{j,k}^h| &:= |\langle f^h, \tilde{\psi}_{j,k} \rangle| = |\langle f^h - \bar{\pi}, \tilde{\psi}_{j,k} \rangle| \leq \|f^h - \bar{\pi}\|_{L^\infty(\tilde{\Sigma}_{j,k})} \|\tilde{\psi}_{j,k}\|_{L^1(\tilde{\Sigma}_{j,k})} \\ &\lesssim |\tilde{\Sigma}_{j,k}|^\mu |f^h|_{W_\infty^\mu(\tilde{\Sigma}_{j,k})} \lesssim 2^{-j\mu} |f^h|_{W_\infty^\mu(\tilde{\Sigma}_{j,k})}, \end{aligned}$$

where $\tilde{\psi}_{j,k}$ is the dual wavelet generated by \mathbf{P}_Λ on the cell $I_{j,k}$. \square

REMARK 2. *Since the spaces W_∞^μ are algebrae, we can infer the regularity of the densities f from the expected regularity of the moments, in particular the conserved ones.*

This inequality⁵ states that the details become small when the function is locally smooth and also that they decrease with the level j if functions are slightly more than just bounded.

3.3. Tree structure and grading. We introduce the set of all indices given by

$$\nabla := \bigcup_{j=\underline{J}}^{\overline{J}} \nabla_j.$$

In order to guarantee the feasibility of all the operations involved with the multiresolution and because it naturally provides a multi-level covering of the domain Ω , we want that our structure $\Lambda \subset \nabla$ represents a graded tree.

DEFINITION 3.5 (Tree). *Let $\Lambda \subset \nabla$ be a set of indices. We say that Λ represents a tree if*

1. *The coarsest level wholly belongs to the structure: $\nabla_{\underline{J}} \subset \Lambda$.*
2. *There is no orphan cell: if $(j, k) \in \Lambda$, then $(j-1, k/2) \in \Lambda$, for $j = \underline{J} + 1, \dots, \overline{J}$.*

Since we have discarded from ∇ the cells having redundant detail, given a tree $\Lambda \subset \nabla$, we consider the complete tree $R(\Lambda)$ obtained by adding the discarded cell with a brother in Λ . With our choice, it is

$$R(\Lambda) = \nabla_{\underline{J}} \cup \{(j, k), (j, k+1) : (j, k) \in \Lambda \text{ for } j = \underline{J} + 1, \dots, \overline{J}\}.$$

Remark that $\Lambda \subsetneq R(\Lambda) \subsetneq \nabla$. We also introduce the set of leaves $L(\Lambda) \subset \Lambda \subset \nabla$ of a tree Λ which is the set of cells without a son. As usual, we introduce the set of complete leaves $S(\Lambda)$ which is given by

$$S(\Lambda) = \{(\underline{J}, k) : (\underline{J}, k) \in L(\Lambda)\} \cup \{(j, k), (j, k+1) : (j, k) \in L(\Lambda) \text{ and } j > \underline{J}\}.$$

As observed by [8], the tree structure and the nesting allow us to conclude that $S(\Lambda)$ is a multi-level partition of the domain Ω . Moreover $L(\Lambda) \subsetneq S(\Lambda) \subsetneq \nabla$. We are ready to provide the definition of graded tree.

DEFINITION 3.6 (Graded tree). *Let $\Lambda \subset \nabla$ be a tree, then it is graded with respect to the prediction operator \mathbf{P}_Λ if the prediction stencil to predict over cells belonging to $R(\Lambda) \setminus \nabla_{\underline{J}}$ also belongs to $R(\Lambda)$. With our prediction operator, this means that*

$$\text{If } (j, k) \in R(\Lambda) \setminus \nabla_{\underline{J}}, \text{ then } (j-1, \lfloor k/2 \rfloor + \delta) \in R(\Lambda), \quad \delta = -\gamma, \dots, \gamma,$$

⁵The interested reader can find a related numerical study in the Supplementary material.

⁶We are sure that $k/2$ is integer because we have only kept even cells

or equivalently, since we have removed redundant odd details

$$\text{If } (j, k) \in \Lambda \setminus \nabla_{\underline{J}}, \text{ then } (j-1, k/2 + \delta) \in R(\Lambda), \quad \delta = -\gamma, \dots, \gamma.$$

Thus, given a tree $\Lambda \subset \nabla$, we denote the operator yielding the smallest graded tree containing Λ as $\mathcal{G}(\Lambda)$. The grading property is important because it guarantees that we can implement the isomorphism between

$$(f_{j,k}^h)_{(j,k) \in S(\Lambda)} \iff (\mathbf{f}_{\underline{J}}^h, (d_{j,k}^h)_{(j,k) \in \Lambda \setminus \nabla_{\underline{J}}}),$$

for every $h = 0, \dots, q-1$ in an efficient manner [8]. This means that it is the same to know the means on the complete leaves $S(\Lambda)$ of a graded tree Λ or knowing the averages on $\nabla_{\underline{J}} \subset \Lambda$ plus the details of $\Lambda \setminus \nabla_{\underline{J}}$. In this work, we choose to store information on the complete leaves $S(\Lambda)$.

Let now $\Lambda \subset \nabla$ be a graded tree and assume to know $(f_{j,k}^h)_{(j,k) \in S(\Lambda)}$ or equivalently $(\mathbf{f}_{\underline{J}}^h, (d_{j,k}^h)_{(j,k) \in \Lambda \setminus \nabla_{\underline{J}}})$ for every $h = 0, \dots, q-1$. From this information, we can build the reconstruction

$$\widehat{\widehat{\mathbf{f}}}_{\underline{J}}^h := \left(\widehat{\widehat{f}}_{\underline{J},k}^h \right)_{k=0, \dots, N_{\underline{J}-1}},$$

for $h = 0, \dots, q-1$, where the double hat represents the recursive application of the prediction operator \mathbf{P}_{Λ} without adding the details (indeed, not available) until reaching the complete leaves $S(\Lambda)$ on which information is stored.

3.4. Compressing information. Take a graded tree $\Lambda \subset \nabla$, then we consider the thresholding (or coarsening) operator given by

$$\mathcal{T}_{\epsilon}(\Lambda) := \nabla_{\underline{J}} \cup \left\{ (j, k) \in \Lambda \setminus \nabla_{\underline{J}} : \max_{h=0, \dots, q-1} |d_{j,k}^h| \geq \epsilon_j \right\} \subset \nabla,$$

where the details concern $(f_{j,k}^h)_{(j,k) \in S(\Lambda)}$ for $h = 0, \dots, q-1$. This operator is constructed to work with the same discretization for all the fields spanned by h . It can be shown [8, 16] that

PROPOSITION 3.7. *Let $\epsilon > 0$ and consider a graded tree $\Lambda \subset \nabla$ with data known on its complete leaves $S(\Lambda)$. Consider the choice of level-wise thresholds*

$$\epsilon_j = 2^{j-\bar{J}}\epsilon, \quad j = \underline{J} + 1, \dots, \bar{J},$$

and consider $p \in [0, \infty]$. Then there exists a constant $C_{MR} = C_{MR}(\gamma, p) > 0$ independent of L such that

$$\left\| \widehat{\widehat{\mathbf{f}}}_{\underline{J}}^h - \mathbf{A}_{\mathcal{G} \circ \mathcal{T}_{\epsilon}(\Lambda)} \widehat{\widehat{\mathbf{f}}}_{\underline{J}}^h \right\|_{\ell^p} \leq C_{MR}\epsilon,$$

for every $h = 0, \dots, q-1$, where $\mathbf{A}_{\Lambda} := \mathcal{M}_{\mathcal{R}}^{-1} T_{\Lambda} \mathcal{M}_{\mathcal{R}}$, where T_{Λ} is the operator putting the details corresponding to indices which do not belong to Λ to zero.

A similar estimate clearly holds when gathering all the populations spanning $h = 0, \dots, q-1$. It means that we can discard cells with small details still being able to reconstruct at the finest level \bar{J} within a given precision controlled by ϵ . We can then rely on this machinery in order to conduct a compression process and build a numerical strategy based on LBM schemes.

4. Adaptive MR-LBM scheme and error control. So far, the procedure based on the multiresolution is static with respect to the evolution of time. Since we want to utilize this strategy to build a reliable fully adaptive lattice Boltzmann solver for time dependent problems, it is of the foremost importance to define a way of evolving the compressed mesh so that it correctly represents the solution both at current time t^n and at the successive time t^{n+1} , constructing it without *a priori* knowing the new solution.

4.1. Mesh adaptation strategy and time-stepping. We are given an adaptive graded tree $\Lambda^n \subset \nabla$ and a solution $(f_{j,k}^{h,n})_{(j,k) \in S(\Lambda^n)}$ for $h = 0, \dots, q-1$ defined on the complete leaves of Λ^n for the discrete time t^n .

4.1.1. Mesh adaptation. Starting from this level of information, which yields $(\underline{f}_{\underline{j}}^{h,n}, (d_{j,k}^{h,n})_{(j,k) \in \Lambda^n \setminus \nabla_{\underline{j}}})$ using \mathbf{P}_{\wedge} and \mathbf{P}_{\vee} , we want to create a new mesh Λ^{n+1} used to compute the new solution at time t^{n+1} on $S(\Lambda^{n+1})$. The procedure can be schematized as follows

$$\Lambda^{n+1} := \mathcal{G} \circ \mathcal{H}_{\epsilon} \circ \mathcal{T}_{\epsilon}(\Lambda^n),$$

where the details used by \mathcal{H}_{ϵ} (still to be defined) and \mathcal{T}_{ϵ} are those of the old solution, namely $(d_{j,k}^{h,n})_{(j,k) \in \Lambda^n \setminus \nabla_{\underline{j}}}$. In the previous expression, we have:

- \mathcal{T}_{ϵ} is the thresholding operator we have previously defined. It can only merge fine cells on the tree to form coarser ones (coarsen).
- \mathcal{H}_{ϵ} is the enlargement operator. It breaks cells to form finer ones (refines) and is constructed to slightly enlarge the structure in order to accommodate the slowly evolving solution at the new time t^{n+1} .
- \mathcal{G} is the grading operator, which can also refine.

Once we have Λ^{n+1} , we adapt the solution from $S(\Lambda^n)$ to $S(\Lambda^{n+1})$. When passing from Λ^n to Λ^{n+1} , if cells are coarsened, we have to merge their data with the projection operator \mathbf{P}_{\vee} . On the other hand, when finer cells are added by \mathcal{H}_{ϵ} or \mathcal{G} , the missing information is reconstructed using the prediction operator \mathbf{P}_{\wedge} . We are left with the old solution at time t^n on the complete leaves of the new mesh $S(\Lambda^{n+1})$: $(f_{j,k}^{h,n})_{(j,k) \in S(\Lambda^{n+1})}$ for $h = 0, \dots, q-1$.

4.1.2. Time-stepping. We denote the operator associated with the adaptive MR-LBM scheme by \mathbf{L}_A^n (described in the sequel), with explicit dependence on the time t^n since acting only on data defined on the time varying $S(\Lambda^{n+1})$. It gives the approximate solution at time t^{n+1} on the same hybrid grid. This is

$$\left(f_{j,k}^{h,n+1} \right)_{\substack{(j,k) \in S(\Lambda^{n+1}) \\ h=0, \dots, q-1}} = \mathbf{L}_A^n \left(f_{j,k}^{h,n} \right)_{\substack{(j,k) \in S(\Lambda^{n+1}) \\ h=0, \dots, q-1}}.$$

4.2. Construction of the enlargement operator \mathcal{H}_{ϵ} . We still have to define the enlargement operator \mathcal{H}_{ϵ} , which is based on the following principles:

- We must ensure that the propagation of information at finite speed *via* the stencil of the lattice Boltzmann operator \mathbf{L} (and thus also \mathbf{L}_A^n) is correctly handled. Thus, setting $\sigma = \max_{h=0, \dots, q-1} |w^h|$, we enforce that:

$$\text{If } (j, k) \in R(\mathcal{T}_{\epsilon}(\Lambda^n)), \quad \text{then } (j, k + \delta) \in R(\mathcal{H}_{\epsilon} \circ \mathcal{T}_{\epsilon}(\Lambda^n)), \quad \delta = -\sigma, \dots, \sigma,$$

- We must detect the shock formation possibly induced by the non linearity of

the collisional part of \mathbf{L} (or \mathbf{L}_A^n). Consider $\bar{\mu} \geq 0$ to be tuned, then

$$(4.1) \quad \begin{aligned} & \text{If } (j, k) \in \mathcal{T}_\epsilon(\Lambda^n), \quad \underline{J} < j < \bar{J}, \quad \text{and} \quad \max_{h=0, \dots, q-1} |d_{j,k}^{h,n}| \geq 2^{\bar{\mu}+1} \epsilon_j, \\ & \text{then } (j+1, 2k+\delta) \in R(\mathcal{H}_\epsilon \circ \mathcal{T}_\epsilon(\Lambda^n)), \quad \delta = 0, 1, 2, 3. \end{aligned}$$

The rationale is the following: assume that the function $f^h(t^{n+1}, x)$ corresponding to $(f_{j,k}^{h,n+1})_{(j,k) \in S(\Lambda^{n+1})}$ is such that $f^h(t^{n+1}, \cdot) \in W_\infty^\nu(\tilde{\Sigma}_{j,k})$ for some $\nu \geq 0$. Set $\bar{\mu} = \min(\nu, \mu)$. Since this solution is unknown at the stage at which we are utilizing \mathcal{H}_ϵ , we assume that the solution varies slowly from t^n to t^{n+1} , so that we claim

$$|d_{j,k}^{h,n+1}| \approx |d_{j,k}^{h,n}| \approx 2^{-j\bar{\mu}} |f^h(t^n, \cdot)|_{W_\infty^{\bar{\mu}}(\tilde{\Sigma}_{j,k})}$$

using (3.3) and for the details which may not be available in the structure

$$\begin{aligned} |d_{j+1,2k}^{h,n+1}| &\approx |d_{j+1,2k}^{h,n}| \approx 2^{-(j+1)\bar{\mu}} |f^h(t^n, \cdot)|_{W_\infty^{\bar{\mu}}(\tilde{\Sigma}_{j+1,2k})}, \\ &\leq 2^{-(j+1)\bar{\mu}} |f^h(t^n, \cdot)|_{W_\infty^{\bar{\mu}}(\tilde{\Sigma}_{j,k})}, \end{aligned}$$

using the nesting of the lattices. As a consequence, we have

$$(4.2) \quad |d_{j+1,2k}^{h,n+1}| \approx 2^{-\bar{\mu}} |d_{j,k}^{h,n}|.$$

According to the analysis to construct the truncation operator $\mathcal{T}_\epsilon(\Lambda^{n+1})$ ⁷, we would have kept $I_{j+1,2k}$ and $I_{j+1,2k+1}$ if $|d_{j+1,2k}^{h,n+1}| \geq \epsilon_{j+1} = 2\epsilon_j$ and a priori also $I_{j+1,2k+2}$ and $I_{j+1,2k+3}$, because their father has a detail with the same absolute value of its brother. This comes back, using the previous estimate, at doing so whenever $|d_{j,k}^{h,n}| \geq 2^{\bar{\mu}+1} \epsilon_j$. Since the local regularity ν of the solution at each time step is unknown, $\bar{\mu} = \min(\nu, \mu)$ is a parameter of the simulation to be set.

Modulo this operation on the mesh, which slightly enlarges the set of kept cells, we claim that the following heuristics, inspired by the works of Harten [31], holds:

ASSUMPTION 1 (Harten heuristics). *The tree $\mathcal{T}_\epsilon(\Lambda^n)$ has been enlarged into a graded tree $\Lambda^{n+1} = \mathcal{G} \circ \mathcal{H}_\epsilon \circ \mathcal{T}_\epsilon(\Lambda^n)$ such that for the chosen $p \in [1, \infty]$*

$$\left\| \widehat{\mathbf{f}}_{\bar{J}}^n - \mathbf{A}_{\Lambda^{n+1}} \widehat{\mathbf{f}}_{\bar{J}}^n \right\|_{\ell^p} \leq C_{MR} \epsilon, \quad \left\| \widehat{\mathbf{L}} \widehat{\mathbf{f}}_{\bar{J}}^n - \mathbf{A}_{\Lambda^{n+1}} (\widehat{\mathbf{L}} \widehat{\mathbf{f}}_{\bar{J}}^n) \right\|_{\ell^p} \leq C_{MR} \epsilon.$$

The first assumption inequality is naturally fulfilled using the fact that $\mathcal{T}_\epsilon(\Lambda^n) \subset \Lambda^{n+1}$. The second inequality is verified upon having enlarged the mesh using \mathcal{H}_ϵ , which has been built considering how the scheme operator \mathbf{L} acts on the solution. It basically means that the mesh is suitable for well representing the solution obtained by applying the reference scheme to the adaptive solution at the previous time step t^n reconstructed on the finest level.

4.3. Construction of the adaptive MR-LBM scheme. We now present how to construct the adaptive MR-LBM scheme \mathbf{L}_A^n from the reference scheme \mathbf{L} .

⁷ $n+1$ because we are trying to anticipate the evolution of the solution.

4.3.1. Collision. In this part, the change of variable *via* \mathbf{M} is understood. We reconstruct the data on the finest mesh $\mathcal{L}_{\bar{J}}$, we perform the collision and then project back on the complete leaves $S(\Lambda^{n+1})$. Let $(j, k) \in S(\Lambda^{n+1})$, then

$$(4.3) \quad m_{j,k}^{h,n\star} = m_{j,k}^{h,n}, \quad h = 0, \dots, q_{\text{cons}} - 1,$$

$$m_{j,k}^{h,n\star} = (1 - s^h) m_{j,k}^{h,n} + \frac{s^h}{2^{\bar{J}-j}} \sum_{\delta=0}^{2^{\bar{J}-j}-1} M^{h,\text{eq}} \left(\widehat{m}_{\bar{J},k2^{\bar{J}-j+\delta}}^{0,n}, \dots, \widehat{m}_{\bar{J},k2^{\bar{J}-j+\delta}}^{q_{\text{cons}}-1,n} \right),$$

for $h = q_{\text{cons}}, \dots, q - 1$.

REMARK 3. *As observed by [35] for the source terms of Finite Volumes schemes, this strategy yields can be really computationally costly and is mostly of theoretical interest. We shall discuss this fact and introduce an alternative approach in the sequel.*

The first term on the right is taken on the complete leaf because it is linear, thus the reconstructed values simplify when taking the projection operator.

4.3.2. Stream. For the sake of notation, let us introduce the sign of each velocity given by $\sigma^h := w^h/|w^h| \in \{-1, 0, 1\}$ for $h = 0, \dots, q - 1$ fixed in the sequel. Consider a complete leaf $(j, k) \in S(\Lambda^{n+1})$. Consider all the cells of $\mathcal{L}_{\bar{J}}$ inside $I_{j,k}$ with indices $(\bar{J}, k2^{\bar{J}-j} + \delta)$ with $\delta = 0, \dots, 2^{\bar{J}-j} - 1$. Perform the advection on them

$$f_{\bar{J},k2^{\bar{J}-j+\delta}}^{h,n+1} = f_{\bar{J},k2^{\bar{J}-j+\delta-w^h}}^{h,n\star}, \quad \text{for } \delta = 0, \dots, 2^{\bar{J}-j} - 1.$$

The problem is that the data on the right hand side are usually unavailable since since their cell does not belong to $S(\Lambda^{n+1})$. Despite this, we can reconstruct, yielding

$$f_{\bar{J},k2^{\bar{J}-j+\delta}}^{h,n+1} \approx \widehat{f}_{\bar{J},k2^{\bar{J}-j+\delta-w^h}}^{h,n\star}, \quad \text{for } \delta = 0, \dots, 2^{\bar{J}-j} - 1.$$

We want to update the solution on $S(\Lambda^{n+1})$, that is why we project using $\bar{J} - j$ times the projection operator \mathbf{P}_{\vee}

$$(4.4) \quad f_{\bar{J},k2^{\bar{J}-j+\delta}}^{h,n+1} \approx \frac{1}{2^{\bar{J}-j}} \sum_{\delta=0}^{2^{\bar{J}-j}-1} \widehat{f}_{\bar{J},k2^{\bar{J}-j+\delta-w^h}}^{h,n\star}.$$

Indeed, only the terms referring to the virtual cells close to the boundary of the leaf are actually needed. After tedious but straightforward computations, setting $\eta(h, \delta) := (1/2 - \delta)\sigma^h - 1/2 \in \mathbb{Z}$ for $\delta = 1, \dots, |w^h|$, we come to

$$(4.5) \quad f_{\bar{J},k2^{\bar{J}-j+\delta}}^{h,n+1} \approx f_{\bar{J},k2^{\bar{J}-j+\delta}}^{h,n\star} + \frac{\sigma^h}{2^{\bar{J}-j}} \sum_{\delta=0}^{|w^h|} \left(\widehat{f}_{\bar{J},k2^{\bar{J}-j+\eta(h,\delta)}}^{h,n\star} - \widehat{f}_{\bar{J},(k+1)2^{\bar{J}-j+\eta(h,\delta)}}^{h,n\star} \right).$$

REMARK 4. *Since the reconstruction operator \approx which utilizes \mathbf{P}_{\wedge} until reaching available values on $S(\Lambda^{n+1})$ does not depend on the details (they are not available) one might use cheaper interpolation to perform this operation, as hinted by [8]. Such an approach is used in many works, but at the cost of the error control provided by the MR machinery.*

4.4. Error analysis. The major interest of adaptive meshes generated by multiresolution is that we can recover a precise error control on the additional error when

solving PDEs on them. Fixing a given ℓ^p norm for $p \in [1, \infty]$, we want to control the additional error $\|\mathbf{F}^n - \widehat{\mathbf{f}}^n\|_{\ell^p}$, where \mathbf{F}^n is the solution of the reference scheme given by $\mathbf{F}^{n+1} = \mathbf{L}\mathbf{F}^n$ and computations start from the same initial datum on the finest grid, that is $\Lambda^0 = \nabla$. In the following analysis, the assumptions are the following

- **H1 - Harten heuristics.** At each step, the tree $\mathcal{T}_\epsilon(\Lambda^n)$ has been enlarged into a graded tree Λ^{n+1} so that

$$\left\| \widehat{\mathbf{f}}_{\mathcal{J}}^n - \mathbf{A}_{\Lambda^{n+1}} \widehat{\mathbf{f}}_{\mathcal{J}}^n \right\|_{\ell^p} \leq C_{\text{MR}} \epsilon, \quad \left\| \mathbf{L} \widehat{\mathbf{f}}_{\mathcal{J}}^n - \mathbf{A}_{\Lambda^{n+1}} (\mathbf{L} \widehat{\mathbf{f}}_{\mathcal{J}}^n) \right\|_{\ell^p} \leq C_{\text{MR}} \epsilon.$$

- **H2 - Continuity of \mathbf{L} .** There exists a constant $C_L = 1 + \tilde{C}_L$ with $\tilde{C}_L \geq 0$ such that

$$\|\mathbf{L}\mathbf{F} - \mathbf{L}\mathbf{G}\|_{\ell^p} \leq C_L \|\mathbf{F} - \mathbf{G}\|_{\ell^p}, \quad \forall \mathbf{F}, \mathbf{G} \in \mathbb{R}^{qN_{\mathcal{J}}}.$$

REMARK 5. *The following procedure can be easily adapted to the context where the continuity of the scheme is measured using a ℓ^2 -weighted norm as by [37]. It is sufficient to consider $p = 2$ and to observe that the corresponding norm (measuring the properties pertaining to the multiresolution) can be bounded by the ℓ^2 -weighted norm.*

Thus we prove the following statement which gives a control on the error introduced by the MR-LBM adaptive scheme:

PROPOSITION 4.1 (Additional error estimate). *Under the Assumptions (H1) and (H2), the additional error satisfies the following upper bounds*

$$\|\mathbf{F}^n - \widehat{\mathbf{f}}^n\|_{\ell^p} \leq C_{\text{MR}} \epsilon \times \begin{cases} n+1, & \text{if } \tilde{C}_L = 0, \\ 1 + \frac{e^{\tilde{C}_L n} - 1}{\tilde{C}_L}, & \text{if } \tilde{C}_L > 0. \end{cases}$$

Proof. Start by observing that as stated by (5.3) in [8], by (H1) we can claim that

$$(4.6) \quad \widehat{\mathbf{f}}^{n+1} = (\mathbf{A}_{\Lambda^{n+1}} \circ \mathbf{L}) \widehat{\mathbf{f}}^n.$$

Hence by the triangle inequality

$$\begin{aligned} \|\mathbf{F}^n - \widehat{\mathbf{f}}^n\|_{\ell^p} &\leq \|\mathbf{L}\mathbf{F}^{n-1} - \mathbf{L}\widehat{\mathbf{f}}^{n-1}\|_{\ell^p} + \|\mathbf{L}\widehat{\mathbf{f}}^{n-1} - \widehat{\mathbf{f}}^n\|_{\ell^p}, \\ &\leq (1 + \tilde{C}_L) \|\mathbf{F}^{n-1} - \widehat{\mathbf{f}}^{n-1}\|_{\ell^p} + \|\mathbf{L}\widehat{\mathbf{f}}^{n-1} - (\mathbf{A}_{\Lambda^n} \circ \mathbf{L}) \widehat{\mathbf{f}}^{n-1}\|_{\ell^p}, \\ &\leq (1 + \tilde{C}_L) \|\mathbf{F}^{n-1} - \widehat{\mathbf{f}}^{n-1}\|_{\ell^p} + C_{\text{MR}} \epsilon, \end{aligned}$$

employing in this order Assumption (H2), (4.6) and Assumption (H1). We have to distinguish two cases and apply the inequality recursively

- $\tilde{C}_L = 0$, thus $\|\mathbf{F}^n - \widehat{\mathbf{f}}^n\|_{\ell^p} \leq \|\mathbf{F}^{n-1} - \widehat{\mathbf{f}}^{n-1}\|_{\ell^p} + C_{\text{MR}} \epsilon \leq \dots \leq C_{\text{MR}}(n+1)\epsilon$.
- $\tilde{C}_L > 0$. We obtain, using that $(1 + \tilde{C})^n \leq e^{\tilde{C}n}$ if $\tilde{C} > 0$

$$\begin{aligned} \|\mathbf{F}^n - \widehat{\mathbf{f}}^n\|_{\ell^p} &\leq (1 + \tilde{C}_L) \|\mathbf{F}^{n-1} - \widehat{\mathbf{f}}^{n-1}\|_{\ell^p} + C_{\text{MR}} \epsilon \leq \dots \\ &\leq C_{\text{MR}} \epsilon \sum_{i=0}^{n-1} (1 + \tilde{C}_L)^i + C_{\text{MR}} \epsilon = C_{\text{MR}} \left(1 + \frac{(1 + \tilde{C}_L)^n - 1}{\tilde{C}_L} \right) \epsilon \\ &\leq C_{\text{MR}} \left(1 + \frac{e^{\tilde{C}_L n} - 1}{\tilde{C}_L} \right) \epsilon. \quad \square \end{aligned}$$

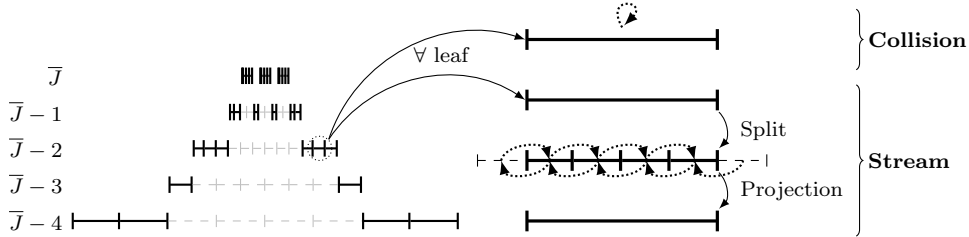


FIG. 3. Schematic illustration of the basic features of the adaptive numerical scheme as it is currently used in the paper, meaning with the “leaves collision” (4.7).

Therefore, regardless of continuity constant of the reference scheme, the additional error is bounded linearly with ϵ . According to the value of constant, we can prove that it accumulates either at most linearly in time or exponentially.

4.5. Conclusion, discussion and implementation. As we observed with Remark 3, the collision given by (4.3) (called “reconstructed collision”) is used in the theoretical analysis but remains limiting in practice, especially in the multidimensional context [1]. Therefore, we propose the so-called “leaves collision” (see Figure 3), using data available on the complete leaves $S(\Lambda^{n+1})$. This reads, for $(j, k) \in S(\Lambda^{n+1})$

$$(4.7) \quad \begin{aligned} m_{j,k}^{h,n^*} &= m_{j,k}^{h,n}, \quad h = 0, \dots, q_{\text{cons}} - 1, \\ m_{j,k}^{h,n^*} &= (1 - s^h)m_{j,k}^{h,n} + s^h M^{h,\text{eq}} \left(m_{j,k}^{0,n}, \dots, m_{j,k}^{q-1,n} \right), \quad h = q_{\text{cons}}, \dots, q - 1. \end{aligned}$$

This is significantly cheaper than (4.3) because there is no need to reconstruct a piecewise constant representation of the solution on the full finest level. Moreover, in the case where the equilibria are linear, we are still able to prove Proposition 4.1 and we might argue that in practice it is still verified for non-linear cases. We shall validate this claim with simulations and provide an *ad-hoc* pathological example where the Proposition 4.1 does not hold, with full discussion in the Supplementary material.

For the stream phase, even if we reconstruct at the finest level, the computation can be done at minimal expenses because we are capable of passing from (4.4) to (4.5) by linearity. Using cheaper reconstruction operators as hinted by Remark 4 cannot yield the control by Proposition 4.1 and we have verified that it frequently generates low-quality results. This is the subject of a future contribution.

The algorithms are sequentially implemented in C++ using a code called SAMURAI⁸ (Structured Adaptive mesh and Multi-Resolution based on Algebra of Intervals) which is currently under development and that can handle general problems involving dynamically refined meshes (both MR and AMR). The central features of SAMURAI are its data structure based on intervals of contiguous cells along each axis and an ensemble of set operations to quickly and easily perform inter-level operations.

5. Verifications. In this Section, we concentrate on two main aspects, namely:

- The fulfillment of the theoretical estimate by Proposition 4.1⁹ The errors are measured on the conserved moments. In particular, we look at:

$$E^{h,n} := \|\mathbf{M}^{h,\text{ex}}(t^n) - \mathbf{M}^{h,n}\|_{\ell^1}, \quad e^{h,n} := \|\mathbf{M}^{h,n} - \widehat{\widehat{\mathbf{m}}}_J^{h,n}\|_{\ell^1},$$

⁸Code, test cases and documentation available at <https://github.com/hpc-maths/samurai>.

⁹Even when we are not able to verify the continuity property of the reference scheme.

for $h = 0, \dots, q_{\text{cons}} - 1$, which are respectively the error of the reference method against the exact solution and the difference between the adaptive solution and the reference solution.

- The gain in terms of computational time induced by the use of multiresolution. In this work, we use the compression factor, which is given by $100 \times (1 - \sharp(S(\Lambda^n))/N_{\bar{J}})$, as a measure of computational efficiency, knowing that the real one is strongly dependent on the implementation and data structure and will be studied in future works.

Unless otherwise stated, the test are carried using the “leaves collision”. An exception to this rule is presented in details in the Supplementary material.

5.1. D_1Q_2 for a scalar conservation law: advection and Burgers equations.

5.1.1. The problem and the scheme. We aim at approximating the weak entropic solution (see Serre [46]) of the initial-value problem:

$$(5.1) \quad \begin{cases} \partial_t \rho + \partial_x(\varphi(\rho)) = 0, & t \in [0, T], & x \in \mathbb{R}, \\ \rho(t = 0, x) = \rho_0(x), & & x \in \mathbb{R}. \end{cases}$$

with $\varphi \in C^\infty(\mathbb{R})$ a flux and $\rho_0 \in L^\infty(\mathbb{R})$. This problem is the advection equation with constant velocity for $\varphi(\xi) = c\xi$ with velocity $c \in \mathbb{R}$ and the inviscid Burgers equation for $\varphi(\xi) = \xi^2/2$. The D_1Q_2 scheme is obtained by selecting $q = 2$ and $q_{\text{cons}} = 1$ with velocities $v^0 = \lambda$, $v^1 = -\lambda$ and change of basis

$$M = \begin{pmatrix} 1 & 1 \\ \lambda & -\lambda \end{pmatrix}.$$

With the theory of equivalent equations [20], Graille [29] has shown that the equivalent equation for this scheme is (5.1) up to first order in Δt upon selecting $M^{1,\text{eq}} = \varphi(M^0)$.

EXAMPLE 1. *In the case of advection equation with $\lambda \geq c > 0$, we have an explicit expression for the optimal continuity constant of the scheme for the ℓ^1 norm, namely $C_L = 1$ if $s \leq 2/(1 + c/\lambda)$ or $C_L = s(1 + c/\lambda) - 1$ otherwise.*

TABLE 1

Test cases for one scalar conservation law with choice of flux, initial datum, expected regularity of the solution, choice of the regularity parameter $\bar{\mu}$ and final time of the simulation.

Flux φ	Initial datum ρ_0	Type of solution	$\bar{\mu}$	T	Test
$\varphi(u) = \frac{3}{4}u$	$\rho_0(x) = e^{-20x^2}$	Strong C^∞	∞	0.4	I
	$\rho_0(x) = \chi_{ x < 1/2}(x)$	Weak L^∞	0	0.4	II
$\varphi(u) = \frac{u^2}{2}$	$\rho_0(x) = (1 + \tanh(100x))/2$	Strong C^∞	∞	0.4	III
	$\rho_0(x) = \chi_{ x \leq 1/2}(x)$	Weak L^∞	0	0.7	IV
	$\rho_0(x) = (1 + x)\chi_{x < 0}(x) + (1 - x)\chi_{x > 0}(x)$	Weak L^∞	0	1.3	V

5.1.2. Results. For this test case, we consider $\Omega = [-3, 3]$, $\underline{J} = 2$, $\bar{J} = 9$, $\gamma = 1$ and $\epsilon = 1e - 4$ unless otherwise said. Concerning the lattice Boltzmann scheme, we fix $\lambda = 1$ and we vary the relaxation parameter. The tests we perform are resumed on Table 1. In order not to overcharge the paper with plots, we just provide the values for the ratio $E^{0,N}/e^{0,N}$ at final time T on Table 2. The time evolution of $e^{0,n}$ as well as that of $E^{0,n}/e^{0,n}$ can be found in the supplementary material. The evolution of the additional error of the adaptive MR-LBM method and the compression factor as

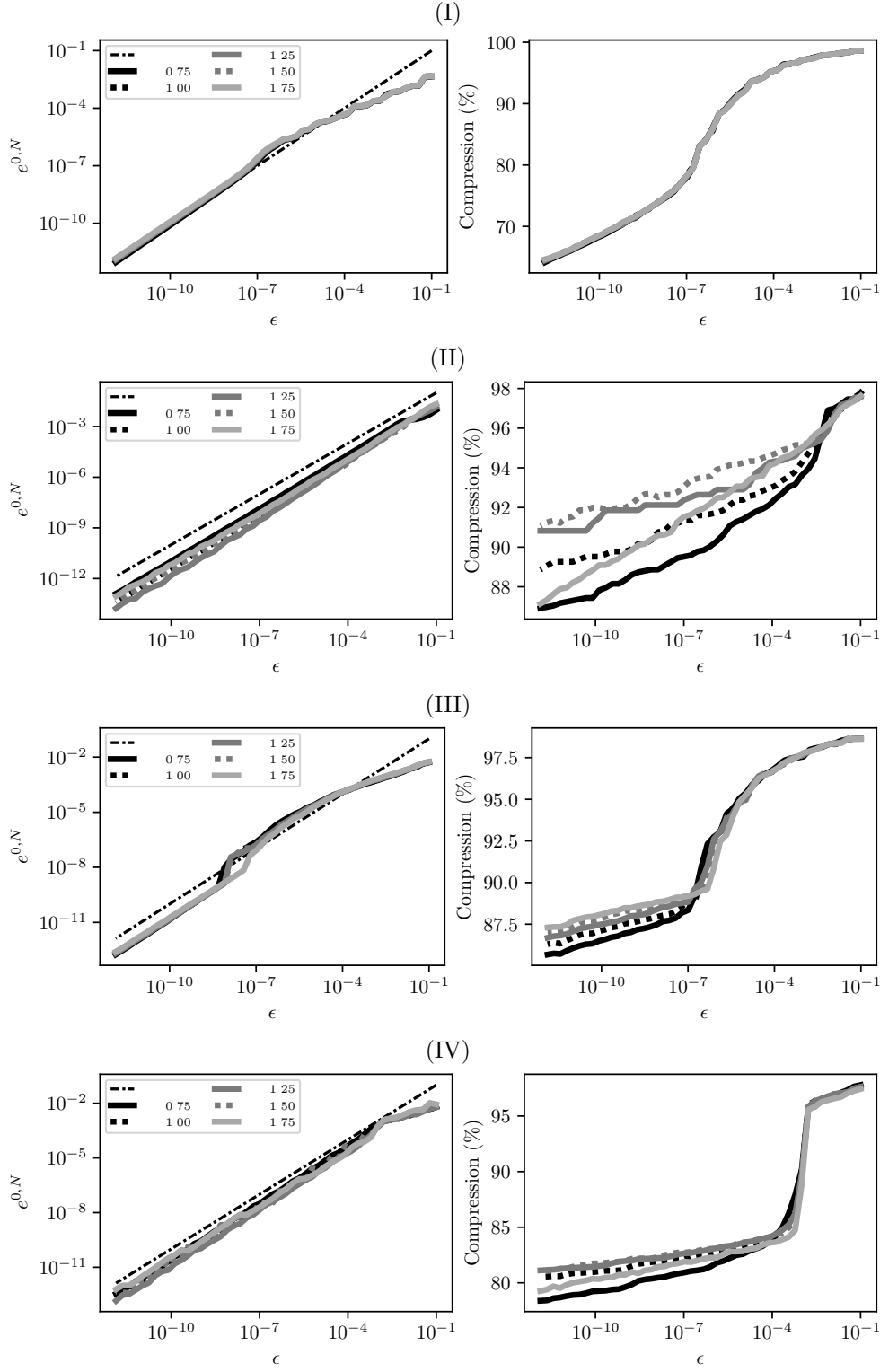


FIG. 4. Behavior of $e^{0,N}$ as function of ϵ (left) and compression factor at the final time as function of ϵ (right), for test (from top to bottom) I, II, III and IV. The dot-dashed line gives the reference $e^{0,N} = \epsilon$.

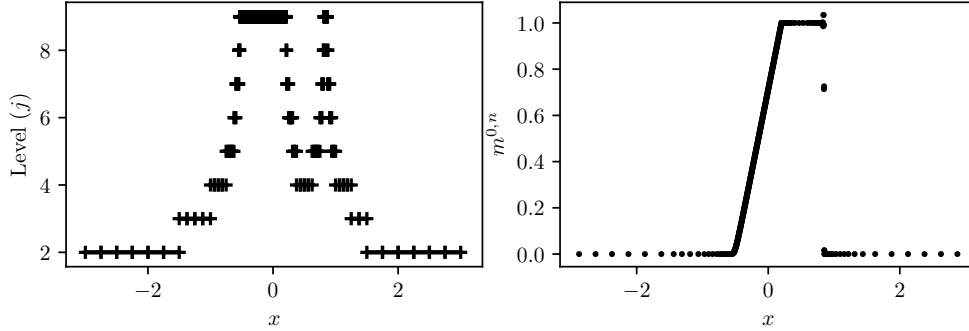


FIG. 5. Example of solution of the D_1Q_2 for the Test IV, considering $n = 358$, $s = 1.5$ and $\epsilon = 10^{-4}$. On the left, levels of the computational mesh. On the right, solution on the leaves of the tree.

TABLE 2

Value of the ratio $E^{0,N}/e^{0,N}$ at final for each test case for one scalar conservation law. The time variation of this quantities can be found in the supplementary material.

s	$E^{0,N}/e^{0,N}$				
	I	II	III	IV	V
0.75	9.97e+01	1.86e+03	5.93e+01	3.50e+02	8.78e+02
1.00	5.94e+01	2.31e+03	3.71e+01	3.41e+02	1.01e+03
1.25	3.52e+01	2.62e+03	2.29e+01	3.93e+02	9.89e+02
1.50	1.94e+01	2.44e+03	1.31e+01	9.72e+01	1.05e+03
1.75	8.34e+00	1.21e+03	5.71e+00	2.90e+02	1.14e+03

function of ϵ are given of Figure 4, except for test number V, which is discussed in more detail in the supplementary material. We formulate the following remarks:

- I. We observe that with this choice of ϵ we successfully keep the additional error by the adaptive MR-LBM scheme $e^{0,n}$ about 10-100 times smaller than the error of the reference scheme $E^{0,n}$, with important compression rates around 95% for the chosen ϵ . We remark the fairly correct linear behavior in terms of ϵ . We have verified that the additional error increases linearly¹⁰ in time even when we can only prove an exponential bound¹¹ by Proposition 4.1.
- II. The error of the adaptive MR-LBM method is about three orders of magnitude smaller than the error of the reference scheme. Due to the presence of large *plateaux*, the compression factor is really interesting for a large range of ϵ , being always over 90%. The trend of $e^{0,N}$ as function of ϵ agrees with the theory and can be bound linearly in time.
- III. Again, we observe that this choice of ϵ grants additional errors which are between 5 and 50 times smaller than the error of the reference method, still preserving excellent compression rates. The behavior as ϵ tends to zero is respected and the expected linear temporal trend is obtained.
- IV. For illustrative purposes the weak solution of the problem is shown on Figure 5). The adaptive method largely beats the traditional method by three orders of magnitude, with less efficient compression compared to (II) due to the formation of a rarefaction fan.¹² The estimate in ϵ is sharply met and the

¹⁰See supplementary material.

¹¹*I.e.* $s > 8/7$.

¹²This rarefaction is straight-shaped but multiresolution refines at the extremal kinks of the slope.

additional error increases linearly in time for every choice of s ¹³.

- V. The outcome of this test is presented and fully discussed in the Supplementary material and provides a pathological example where the reconstructed collision is needed to correctly retrieve the theoretical estimates.

Overall, we can conclude that the adaptive MR-LBM for a scalar conservation law grants an error control by a threshold ϵ and succeeds in keeping the additional error $e^{0,n}$ way smaller than the reference error $E^{0,n}$ (see Table 2) especially when weak solutions are involved. The “leaves collision” does not impact these characteristics except in a specifically designed pathological case.

5.2. D_1Q_3 and D_1Q_5 for two conservation laws: the shallow water system.

5.2.1. The problem and the scheme. We aim at approximating the weak entropic solution of the shallow water system, where h represent the height of a fluid and u is its horizontal velocity:

$$(5.2) \quad \begin{cases} \partial_t h + \partial_x(hu) = 0, & t \in [0, T], & x \in \mathbb{R}, \\ \partial_t(hu) + \partial_x(hu^2 + gh^2/2) = 0, & t \in [0, T], & x \in \mathbb{R}, \\ h(t=0, x) = h_0(x), & & x \in \mathbb{R}, \\ u(t=0, x) = u_0(x), & & x \in \mathbb{R}, \end{cases}$$

where $g > 0$ is the gravitational acceleration exerted on the fluid and $h_0, u_0 \in L^\infty(\mathbb{R})$. Two possible lattice Boltzmann schemes with two conserved moments are:

- D_1Q_3 , obtained selecting $q = 3$ and $q_{\text{cons}} = 2$ with discrete velocities $v^0 = 0$, $v^1 = \lambda$, $v^2 = -\lambda$ and the change of basis:

$$\mathbf{M} = \begin{pmatrix} 1 & 1 & 1 \\ 0 & \lambda & -\lambda \\ 0 & \lambda^2 & \lambda^2 \end{pmatrix}.$$

Selecting $M^{2,\text{eq}} = (M^1)^2/M^0 + g(M^0)^2/2$ the scheme is consistent up to first order in Δt with (5.2).

- D_1Q_5 , obtained taking $q = 5$ and $q_{\text{cons}} = 2$ with the choice of velocities $v^0 = 0$, $v^1 = \lambda$, $v^2 = -\lambda$, $v^3 = 2\lambda$, $v^4 = -2\lambda$, along with the matrix:

$$\mathbf{M} = \begin{pmatrix} 1 & 1 & 1 & 1 & 1 \\ 0 & \lambda & -\lambda & 2\lambda & -2\lambda \\ 0 & \lambda^2 & \lambda^2 & 4\lambda^2 & 4\lambda^2 \\ 0 & \lambda^3 & -\lambda^3 & 8\lambda^3 & -8\lambda^3 \\ 0 & \lambda^4 & \lambda^4 & 16\lambda^4 & 16\lambda^4 \end{pmatrix}.$$

We select the equilibri in the following way:

$$M^{2,\text{eq}} = \frac{(M^1)^2}{M^0} + \frac{g}{2}(M^0)^2, \quad M^{3,\text{eq}} = \alpha\lambda^2 M^1, \quad M^{4,\text{eq}} = \beta\lambda^2 M^{2,\text{eq}},$$

where α and β are real parameters to be set in order to keep the scheme stable. With this choice the equivalent equations are consistent with (5.2) up to first order being close to those of the D_1Q_3 scheme.

Moreover the D_1Q_2 creates a stair-shaped rarefaction, which triggers refinement.

¹³Sometimes with strong oscillations due to the oscillations of the scheme.

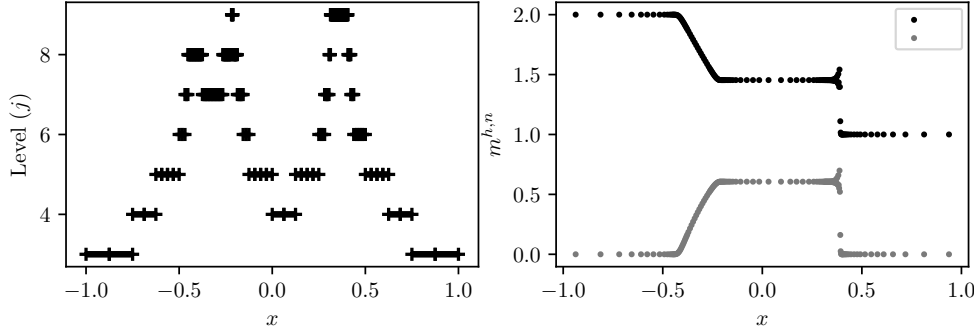


FIG. 6. Example of solution of the D_1Q_5 for the shallow water problem with $n = 300$, $s = 1.6$ and $\epsilon = 10^{-4}$. On the left, levels of the computational mesh. On the right, solution on the leaves of the tree.

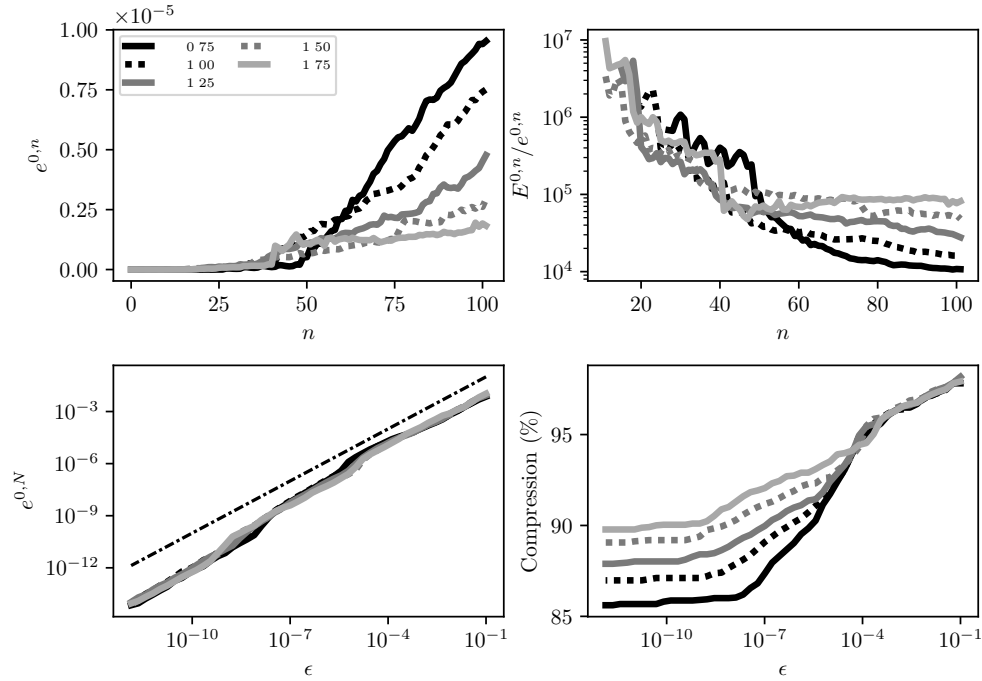


FIG. 7. D_1Q_3 for the shallow water system with Riemann initial datum. The dot-dashed line gives the reference $e^{0,N} = \epsilon$. For the sake of avoiding redundancy, we present only one moment.

5.2.2. Results. As initial datum, we consider the Riemann problem given by $(h_0, u_0)(x) = (2, 0)\chi_{x < 0}(x) + (1, 0)\chi_{x > 0}(x)$, with a lattice velocity $\lambda = 2$, a final time $T = 0.2$ and a domain $\Omega = [-1, 1]$. The result is shown in Figure 7: for both the conserved moments, the behavior of the additional error in time is supra-linear, being very small at the very beginning because the method adds enough security cells around the shock and information propagates relatively slowly. Moreover, we remark that the error is larger for smaller s due to the larger diffusivity of the numerical scheme. The additional error is between four and six orders of magnitude smaller than the error of the reference method, reaching very interesting compression factors.

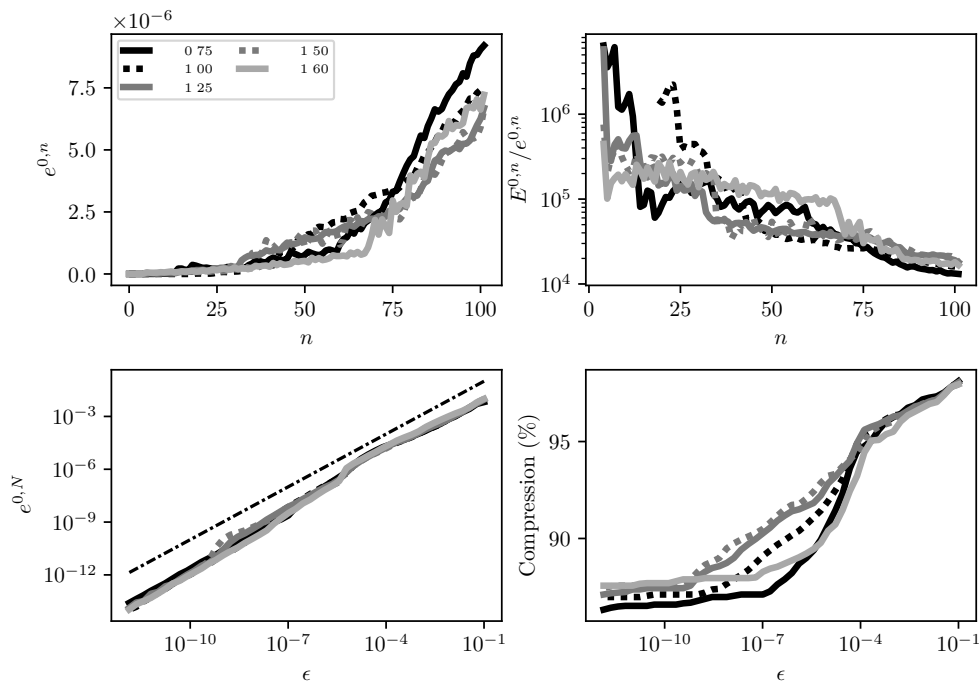


FIG. 8. D_1Q_5 for the shallow water system with Riemann initial datum. The dot-dashed line gives the reference $e^{0,N} = \epsilon$. For the sake of avoiding redundancy, we present only one moment.

The estimates in terms of ϵ are correctly followed.

For the D_1Q_5 , we use exactly the same setting except for taking $\alpha = \beta = 1$ and setting $s_3 = s_4 = 1$. We obtain what is shown in Figures 6 and 8.¹⁴ The time behavior of the additional error is again supra-linear and now the difference between different relaxation parameters is less evident. The ratio with the error of the reference scheme is between 10^4 and 10^6 . The bound in ϵ is very well fulfilled. This example shows that our adaptive strategy works really well even for schemes with an extended advection stencil.

5.3. $D_1Q_2^3$ for the Euler system. We consider the full Euler system

$$(5.3) \quad \begin{cases} \partial_t \rho + \partial_x(\rho u) = 0, & t \in [0, T], & x \in \mathbb{R}, \\ \partial_t(\rho u) + \partial_x(\rho u^2 + p) = 0, & t \in [0, T], & x \in \mathbb{R}, \\ \partial_t E + \partial_x(Eu + pu) = 0, & t \in [0, T], & x \in \mathbb{R}, \\ \rho(t = 0, x) = \rho_0(x), & & x \in \mathbb{R}, \\ u(t = 0, x) = u_0(x), & & x \in \mathbb{R}, \\ E(t = 0, x) = E_0(x), & & x \in \mathbb{R}, \end{cases}$$

where ρ is the density, u the velocity of the flow, p the pressure and E the total energy. The pressure and the energy are linked by the pressure law $E = \rho u^2/2 + p/(\gamma - 1)$. For this work, we consider the Sod shock problem, choosing $\gamma = 1.4$ and considering

¹⁴We are limited to $s = 1.6$ due to stability issues which are inherent to the reference scheme.

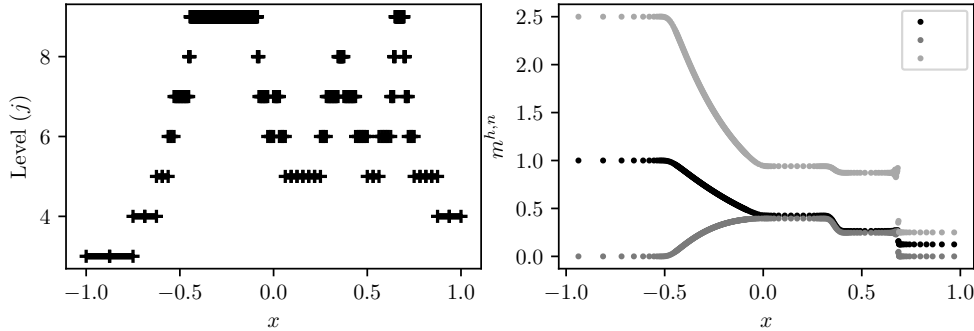


FIG. 9. Example of solution of the vectorial D_1Q_2 for the Sod problem with $n = 600$, $s = 1.75$ and $\epsilon = 10^{-3}$. On the left, levels of the computational mesh. On the right, solution on the leaves of the tree.

the Riemann initial datum given by:

$$(\rho_0, u_0, E_0)(x) = (1.000, 0.000, 2.500)\chi_{x < 0}(x) + (0.125, 0.000, 0.250)\chi_{x > 0}(x),$$

generating a solution with a left-moving rarefaction, a right-moving contact discontinuity and a right-moving shock. We employ a vectorial scheme [29, 21] rather than a scalar one for it adds the necessary numerical diffusion, enhancing stability and it makes easy to conserve E without further manipulation. The scheme is the juxtaposition of three D_1Q_2 for the quantities ρ , ρu and E , coupled through their equilibri:

$$\begin{aligned} M^{1,\text{eq}} &= M^2, & M^{3,\text{eq}} &= \left(\frac{3}{2} - \frac{\gamma}{2}\right) \frac{(M^2)^2}{M^0} + (\gamma - 1)M^4, \\ M^{5,\text{eq}} &= \gamma \frac{M^4 M^2}{M^0} + \frac{1 - \gamma}{2} \frac{(M^2)^3}{(M^0)^2}. \end{aligned}$$

This scheme is consistent up to first order with (5.3) as shown by Graille [29].

5.3.1. Results. We consider a domain $\Omega = [-1, 1]$ and all the other parameters as in the previous examples, except the lattice velocity taken to be $\lambda = 3$ and the final time $T = 0.4$. All the relaxation parameters are taken equal. The result is given in Figures 9 and 10: the additional error behaves fairly linearly in time for every choice of relaxation parameter and becomes smaller as s approaches 2, due to the reduced numerical diffusion. We are capable of keeping the additional error between three and four order of magnitudes smaller than to the error of the reference scheme for each of the conserved moments. The behavior in ϵ is respected. This shows that our strategy is well suited to handle the simulation of systems of conservation laws using vectorial schemes.

6. Conclusions. In this paper, we have presented a class of new fully adaptive lattice Boltzmann schemes based on multiresolution to perform the adaptation of the spatial grid with error control. To the best of our knowledge, no previous research has been conducted to couple multiresolution and LBM methods. The most important features are that there is no need to devise *ad-hoc* refinement/coarsening criteria: mesh adaptation is naturally handled using multiresolution by analyzing the regularity of the solution. Therefore, no previous knowledge of the solution¹⁵ is needed

¹⁵Other than the regularity guess $\bar{\mu}$, which can be set to a small value for precaution.

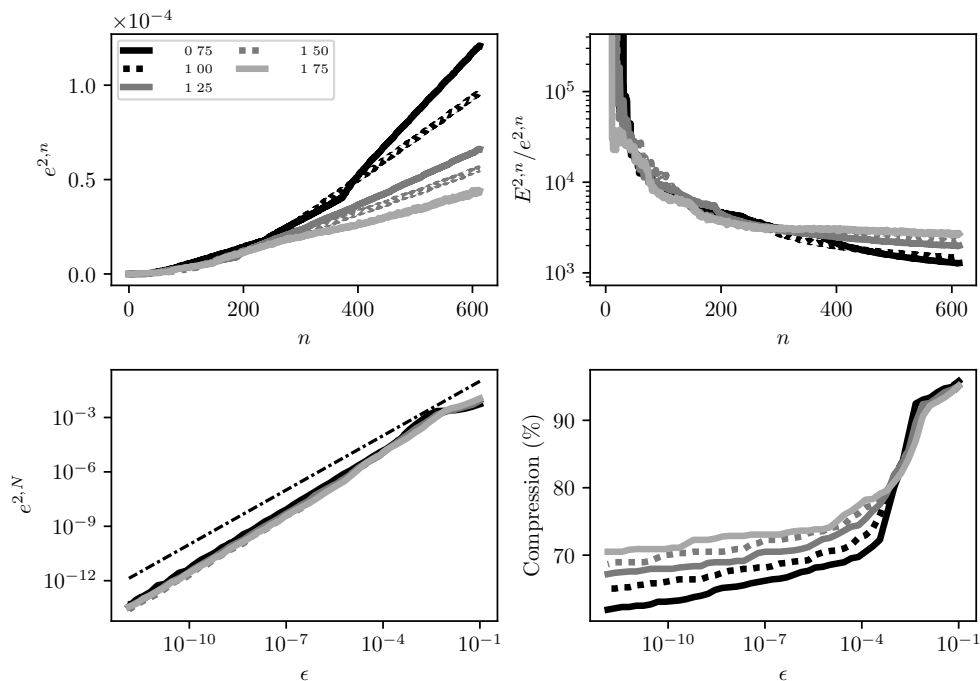


FIG. 10. Vectorial $D_1 Q_2$ for the Sod problem. The dot-dashed line gives the reference $e^{2,N} = \epsilon$. For the sake of compactness, we show only one moment.

because the numerical mesh is automatically evolved. Eventually, under reasonable assumptions on the reference scheme, we are able to prove precise error controls on the additional error introduced by the non-uniform mesh, which are driven by a single adjustable tolerance ϵ . The numerical method has been extensively tested, showing that the theoretical predictions are fully met, even for settings for which we expect less predictable behaviors. We have shown that, by tuning ϵ according to the desired precision, one is capable of keeping the additional error several orders of magnitude below that of the reference method with respect to the exact solution, still achieving excellent compression factors. We have also demonstrated that the optimized “leaves collision” is an efficient alternative to the “reconstructed collision”, except in pathological cases. The question on how the choice of prediction operator could modify the physics approximated by the MR-LBM adaptive scheme will be the object of a forthcoming contribution.

The major improvement our method needs to undergo is its generalization to the multi-dimensional framework (spatial dimension d). We provide answers to this question in a companion contribution [1]. The following points have been taken into consideration:

- The projection operator is straightforwardly generalized as a mean on the children. The prediction operator is constructed by tensor product as hinted by Bihari and Harten [3].
- The decay estimates for the details (3.3) are still valid without having to adjust them with d . Consequently (4.2) remains valid. However, one shall cope with the fact that details of two brothers no longer have the same modulus.
- One must modify the choice of ϵ_j according to d , as the number of elements

in a tree is now bounded by $2^{d\bar{J}}$. We consider $\epsilon_j = 2^{d(j-\bar{J})}\epsilon$. Hence, we need to slightly modify (4.1) which becomes $|d_{j,k}^{h,n}| \geq 2^{\bar{\mu}+d}\epsilon_j$.

- The stream phase given by (4.5) and the way of recovering it remain essentially the same.

In [1], we employ the MR-LBM adaptive scheme to simulate both hyperbolic (Euler) and parabolic (incompressible Navier-Stokes) systems, because the accuracy of our reconstruction is enough to correctly cope with the physics of such systems.

Finally, the optimisation of the implementation is a crucial subject when dealing with multidimensional problems. In this work, we have restricted purposefully the measure of the computational gain with respect to the uniform mesh by merely looking at the compression factor. This is far from realistic if the implementation does not perform the operations involved in multiresolution in a clever way or if the problem is too small to observe a real gain. We believe that the choice of the underlying data structure has a huge impact on this matter: we are currently developing the library SAMURAI with the purpose of providing an innovative interval-based data structure to enhance performances and simplify the parallelization of the whole process. This is the subject of our current research.

7. Acknowledgements. The authors deeply thanks Laurent S eries for fruitful discussions on multiresolution. Thomas Bellotti is supported by a PhD funding (year 2019) from the Ecole polytechnique.

REFERENCES

- [1] T. BELLOTTI, L. GOUARIN, B. GRAILLE, AND M. MASSOT, *A class of multidimensional fully adaptive lattice-boltzmann methods based on multiresolution analysis*, Journal of Computational Physics, (2021). Submitted, available on HAL.
- [2] M. J. BERGER, P. COLELLA, ET AL., *Local adaptive mesh refinement for shock hydrodynamics*, Journal of computational Physics, 82 (1989), pp. 64–84.
- [3] B. L. BIHARI AND A. HARTEN, *Multiresolution schemes for the numerical solution of 2-d conservation laws I*, SIAM Journal on Scientific Computing, 18 (1997), pp. 315–354.
- [4] F. BRAMKAMP, P. LAMBY, AND S. M ULLER, *An adaptive multiscale finite volume solver for unsteady and steady state flow computations*, Journal of Computational Physics, 197 (2004), pp. 460–490.
- [5] R. B URGER, R. RUIZ, K. SCHNEIDER, AND M. A. SEP ULVEDA, *Fully adaptive multiresolution schemes for strongly degenerate parabolic equations with discontinuous flux*, Journal of Engineering Mathematics, 60 (2008), pp. 365–385.
- [6] G. CHIAVASSA AND R. DONAT, *Point value multiscale algorithms for 2D compressible flows*, SIAM J. Sci. Comput., 23 (2001), pp. 805–823.
- [7] A. COHEN, I. DAUBECHIES, AND J.-C. FEAUVEAU, *Biorthogonal bases of compactly supported wavelets*, Communications on pure and applied mathematics, 45 (1992), pp. 485–560.
- [8] A. COHEN, S. KABER, S. M ULLER, AND M. POSTEL, *Fully adaptive multiresolution finite volume schemes for conservation laws*, Mathematics of Computation, 72 (2003), pp. 183–225.
- [9] F. COQUEL, Q. L. NGUYEN, M. POSTEL, AND Q. H. TRAN, *Local time stepping applied to implicit-explicit methods for hyperbolic systems*, Multiscale Modeling & Simulation, 8 (2010), pp. 540–570.
- [10] F. COQUEL, M. POSTEL, N. POUSSINEAU, AND Q.-H. TRAN, *Multiresolution technique and explicit-implicit scheme for multicomponent flows*, Journal of Numerical Mathematics, 14 (2006), pp. 187–216.
- [11] B. CROUSE, E. RANK, M. KRAFczyk, AND J. T OLKE, *A lb-based approach for adaptive flow simulations*, International Journal of Modern Physics B, 17 (2003), pp. 109–112.
- [12] I. DAUBECHIES, *Orthonormal bases of compactly supported wavelets*, Communications on pure and applied mathematics, 41 (1988), pp. 909–996.
- [13] S. DESCOMBES, M. DUARTE, T. DUMONT, F. LAURENT, V. LOUVET, AND M. MASSOT, *Analysis of operator splitting in the nonasymptotic regime for nonlinear reaction-diffusion equations. Application to the dynamics of premixed flames*, SIAM J. Numer. Anal., 52 (2014), pp. 1311–1334.

- [14] R. A. DEVORE AND R. C. SHARPLEY, *Maximal functions measuring smoothness*, vol. 293, American Mathematical Soc., 1984.
- [15] D. D’HUMIÈRES, *Generalized Lattice-Boltzmann Equations*, American Institute of Aeronautics and Astronautics, Inc., 1992, pp. 450–458.
- [16] M. DUARTE, *Adaptive numerical methods in time and space for the simulation of multi-scale reaction fronts*, PhD thesis, Ecole Centrale Paris, 2011. <https://tel.archives-ouvertes.fr/tel-00667857>.
- [17] M. DUARTE, Z. BONAVENTURA, M. MASSOT, AND A. BOURDON, *A numerical strategy to discretize and solve the Poisson equation on dynamically adapted multiresolution grids for time-dependent streamer discharge simulations*, J. Comput. Phys., 289 (2015), pp. 129–148.
- [18] M. DUARTE, S. DESCOMBES, C. TENAUD, S. CANDEL, AND M. MASSOT, *Time-space adaptive numerical methods for the simulation of combustion fronts*, Combustion and Flame, 160 (2013), pp. 1083–1101.
- [19] M. DUARTE, M. MASSOT, S. DESCOMBES, C. TENAUD, T. DUMONT, V. LOUVET, AND F. LAURENT, *New resolution strategy for multiscale reaction waves using time operator splitting, space adaptive multiresolution, and dedicated high order implicit/explicit time integrators*, SIAM Journal on Scientific Computing, 34 (2012), pp. A76–A104.
- [20] F. DUBOIS, *Third order equivalent equation of lattice boltzmann scheme*, Discrete & Continuous Dynamical Systems-A, 23 (2009), p. 221.
- [21] ———, *Simulation of strong nonlinear waves with vectorial lattice boltzmann schemes*, International Journal of Modern Physics C, 25 (2014), p. 1441014.
- [22] T. DUMONT, M. DUARTE, S. DESCOMBES, M.-A. DRONNE, M. MASSOT, AND V. LOUVET, *Simulation of human ischemic stroke in realistic 3D geometry*, Commun. Nonlinear Sci. Numer. Simul., 18 (2013), pp. 1539–1557.
- [23] G. EITEL-AMOR, M. MEINKE, AND W. SCHRÖDER, *A lattice-boltzmann method with hierarchically refined meshes*, Computers & Fluids, 75 (2013), pp. 127–139.
- [24] A. FAKHARI AND T. LEE, *Finite-difference lattice boltzmann method with a block-structured adaptive-mesh-refinement technique*, Physical Review E, 89 (2014), p. 033310.
- [25] Y. FENG, S. GUO, J. JACOB, AND P. SAGAUT, *Grid refinement in the three-dimensional hybrid recursive regularized lattice boltzmann method for compressible aerodynamics*, Phys. Rev. E, 101 (2020), p. 063302.
- [26] O. FILIPPOVA AND D. HÄNEL, *Grid refinement for lattice-bgk models*, Journal of Computational physics, 147 (1998), pp. 219–228.
- [27] C. FORSTER, *Parallel wavelet-adaptive direct numerical simulation of multiphase flows with phase-change*, PhD thesis, Georgia Institute of Technology, 2016.
- [28] F. GENDRE, D. RICOT, G. FRITZ, AND P. SAGAUT, *Grid refinement for aeroacoustics in the lattice boltzmann method: A directional splitting approach*, Phys. Rev. E, 96 (2017), p. 023311.
- [29] B. GRILLE, *Approximation of mono-dimensional hyperbolic systems: A lattice boltzmann scheme as a relaxation method*, Journal of Computational Physics, 266 (2014), pp. 74–88.
- [30] A. HARTEN, *Discrete multi-resolution analysis and generalized wavelets*, Applied numerical mathematics, 12 (1993), pp. 153–192.
- [31] ———, *Adaptive multiresolution schemes for shock computations*, Journal of Computational Physics, 115 (1994), pp. 319–338.
- [32] ———, *Multiresolution algorithms for the numerical solution of hyperbolic conservation laws*, Communications on Pure and Applied Mathematics, 48 (1995), pp. 1305–1342.
- [33] F. J. HIGUERA AND J. JIMÉNEZ, *Boltzmann approach to lattice gas simulations*, EPL (Europhysics Letters), 9 (1989), p. 663.
- [34] J. HORSTMANN, *Hybrid numerical method based on the lattice Boltzmann approach with application to non-uniform grids*, PhD thesis, Université de Lyon, 2018.
- [35] N. HOVHANNISYAN AND S. MÜLLER, *On the stability of fully adaptive multiscale schemes for conservation laws using approximate flux and source reconstruction strategies*, IMA journal of numerical analysis, 30 (2010), pp. 1256–1295.
- [36] H. HUANG, M. SUKOP, AND X. LU, *Multiphase lattice Boltzmann methods: Theory and application*, John Wiley & Sons, 2015.
- [37] M. JUNK AND W.-A. YONG, *Weighted l^2 -stability of the lattice boltzmann method*, SIAM Journal on Numerical Analysis, 47 (2009), pp. 1651–1665.
- [38] P. LALLEMAND AND L.-S. LUO, *Theory of the lattice boltzmann method: Dispersion, dissipation, isotropy, galilean invariance, and stability*, Physical Review E, 61 (2000), p. 6546.
- [39] P. LAMBY, S. MÜLLER, AND Y. STIRIBA, *Solution of shallow water equations using fully adaptive multiscale schemes*, International journal for numerical methods in fluids, 49 (2005), pp. 417–437.

- [40] S. G. MALLAT, *Multiresolution approximations and wavelet orthonormal bases of $l_2(\mathbb{R})$* , Transactions of the American mathematical society, 315 (1989), pp. 69–87.
- [41] G. R. MCNAMARA AND G. ZANETTI, *Use of the boltzmann equation to simulate lattice-gas automata*, Physical review letters, 61 (1988), p. 2332.
- [42] M.-A. N'GUESSAN, *Space adaptive methods with error control based on adaptive multiresolution for the simulation of low-Mach reactive flows*, PhD thesis, Université Paris-Saclay, 2020. <https://tel.archives-ouvertes.fr/tel-02895792>.
- [43] M. N'GUESSAN, M. MASSOT, L. SERIES, AND C. TENAUD, *High order time integration and mesh adaptation with error control for incompressible navier–stokes and scalar transport resolution on dual grids*, Journal of Computational and Applied Mathematics, 387 (2021), p. 112542.
- [44] O. ROUSSEL AND K. SCHNEIDER, *An adaptive multiresolution method for combustion problems: application to flame ball–vortex interaction*, Computers & Fluids, 34 (2005), pp. 817–831.
- [45] O. ROUSSEL, K. SCHNEIDER, A. TSIGULIN, AND H. BOCKHORN, *A conservative fully adaptive multiresolution algorithm for parabolic pdes*, Journal of Computational Physics, 188 (2003), pp. 493–523.
- [46] D. SERRE, *Systems of Conservation Laws 1: Hyperbolicity, entropies, shock waves*, Cambridge University Press, 1999.
- [47] C. TENAUD AND M. DUARTE, *Tutorials on adaptive multiresolution for mesh refinement applied to fluid dynamics and reactive media problems*, in ESAIM: Proceedings, vol. 34, EDP Sciences, 2011, pp. 184–239.
- [48] J. WU AND C. SHU, *A solution-adaptive lattice boltzmann method for two-dimensional incompressible viscous flows*, Journal of Computational Physics, 230 (2011), pp. 2246–2269.

SUPPLEMENTARY MATERIAL
MULTIRESOLUTION-BASED MESH ADAPTATION AND ERROR CONTROL FOR LATTICE BOLTZMANN METHODS WITH APPLICATIONS TO HYPERBOLIC CONSERVATION LAWS

THOMAS BELLOTTI*, LOIĆ GOUARIN*, BENJAMIN GRAILLE†, AND MARC MASSOT*

The aim of this supplementary material is twofold. On one side, in Section 1, we confirm that the estimates on the details decay hold, from an empirical point of view. This is an important fact since they are used throughout the work, in particular to devise the refinement operator \mathcal{H}_ϵ . On the other side, in Section 2, we present and comment additional plots which were left due to space limitations in the main body of the paper. Moreover, we investigate the possible limitations of using the leaves collision instead of the reconstructed collision, showing that the latter is needed only on manufactured pathological cases.

1. Quality of decay estimates to deduce the magnitude of the details.

In this section, we want to verify by numerical experiences that the inequality:

$$(1.1) \quad |d_{j,k}^i| \lesssim 2^{-j \min(\nu, \mu)} |f^i|_{W_\infty^{\min(\nu, \mu)}(\tilde{\Sigma}_{j,k})},$$

is indeed sharp and can be used to predict the magnitude of details which are not available with a good fidelity. In this inequality, ν is the local Sobolev regularity of f^i , meaning that it belongs to W_∞^ν is a neighborhood of the cell $I_{j,k}$ and $\mu = 2\gamma + 1$, where $\gamma \geq 0$ is the size of the prediction stencil. Take four test fields, $\gamma = 1$ (thus $\mu = 3$) and a domain $\Omega = [-3, 3]$:

$$(1.2) \quad \begin{aligned} f^0(x) &= e^{-20x^2}, & f^1(x) &= (1+x)\chi_{[-1,0]}(x) + (1-x)\chi_{[0,1]}(x), \\ f^2(x) &= \sqrt{x}\chi_{[0,1]}(x) + \left(\frac{3}{2} - \frac{x}{2}\right)\chi_{[1,3]}, & f^3(x) &= \frac{1+x}{2}\chi_{[-1,1]}(x), \end{aligned}$$

which have different regularities, namely: $f^0 \in W_\infty^\infty(\Omega)$ (hence $\nu = \infty$), $f^1 \in W_\infty^1(\Omega)$ (hence $\nu = 1$), $f^2 \in W_\infty^{1/2}(\Omega)$ (hence $\nu = 1/2$) and $f^3 \in W_\infty^0(\Omega)$ (hence $\nu = 0$). We consider the detail $d_j^i := \max_k |d_{j,k}^i|$ for the cell where the Sobolev norm is attained, thus maximal, at level j and we look for the ratio with the detail at the finer level $j+1$.

We obtain what is presented in Table 1, showing a very fine agreement with (1.1), meaning that we correctly recover $d_j^i/d_{j+1}^i = 2^{\min(\mu, \nu)}$. We remark that for the most regular function, the size of the details is limited by the choice of prediction operator (μ in this case), whereas for less regular choices, it is the regularity of the function which determines the decay ratio (respectively $\nu = 1, 1/2$ and 0). This confirms the validity of employing (1.1) to devise refinement/coarsening criteria based on multiresolution as we did.

2. Verifications. In this section, concerning the D1Q2 scheme for the solution of a scalar conservation law, we introduce some supplementary figures about the test cases where the leaves collision proved to be effective, namely I, II, III, IV.

*CMAP, CNRS, Ecole polytechnique, Institut Polytechnique de Paris, 91128 Palaiseau Cedex, France. thomas.bellotti@polytechnique.edu

†Institut de Mathématiques d'Orsay, Université Paris-Saclay, 91405 Orsay Cedex, France.

TABLE 1

Empirical detail decay for $\gamma = 1$ for the test cases given by (1.2), measuring the maximum of the detail.

j	$i = 0$		$i = 1$		$i = 2$		$i = 3$	
	d_j^0	d_j^0/d_{j+1}^0	d_j^1	d_j^1/d_{j+1}^1	d_j^2	d_j^2/d_{j+1}^2	d_j^3	d_j^3/d_{j+1}^3
16	4.65e-13	–	3.81e-6	–	4.72e-4	–	1.25e-1	–
15	3.72e-12	8.00	7.63e-6	2.00	6.57e-4	1.39	1.25e-1	1.00
14	2.98e-11	8.00	1.53e-5	2.00	9.23e-4	1.41	1.25e-1	1.00
13	2.38e-10	8.00	3.05e-5	2.00	1.30e-3	1.41	1.25e-1	1.00
12	1.91e-9	8.00	6.10e-5	2.00	1.84e-3	1.41	1.25e-1	1.00
11	1.52e-8	8.00	1.22e-4	2.00	2.60e-3	1.41	1.25e-1	1.00
10	1.22e-7	8.00	2.44e-4	2.00	3.68e-3	1.41	1.25e-1	1.00
9	9.75e-7	8.00	4.88e-4	2.00	5.21e-3	1.41	1.25e-1	1.00
8	7.79e-6	7.99	9.77e-4	2.00	7.37e-3	1.41	1.25e-1	1.00
7	6.22e-5	7.99	1.95e-3	2.00	1.04e-2	1.41	1.25e-1	1.00
6	4.90e-4	7.88	3.91e-3	2.00	1.47e-2	1.41	1.26e-1	1.00
5	3.60e-3	7.35	7.81e-3	2.00	2.08e-2	1.41	1.27e-1	1.01
4	1.96e-2	5.43	1.56e-2	2.00	2.95e-2	1.41	1.29e-1	1.02
3	1.26e-1	6.43	3.13e-2	2.00	4.17e-2	1.41	1.33e-1	1.03
	Theor.	8	Theor.	2	Theor.	$\sqrt{2}$	Theor.	1

Furthermore, we fully describe V, which is constructed in order to warn about the use of the leaves collision.

2.1. D_1Q_2 for a scalar conservation law: advection and Burgers equations.

2.1.1. Tests I, II, III, IV. The information we have not included in the main body of the paper, namely the time behavior of $e^{0,n}$ and of $E^{0,n}/e^{0,n}$ is provided in Figure 1.

It is interesting to observe that the error $e^{0,n}$ accumulates linearly in time as expected. In some cases (especially for IV) some oscillations are present due to the oscillations of the solution close to the shock when using a relaxation parameter $s > 1$. Concerning the ratio $E^{0,n}/e^{0,n}$, one should remark that we have a boundary layer close to the initial time $n = 0$, tending to small values for the regular solutions (I and III) and to very large values ($+\infty$) for the solutions with shocks (II and IV). This can be understood by the fact that at the beginning, when working with Riemann problems, we have added enough security cells around the shock with \mathcal{H}_ϵ and \mathcal{G} in order to make the adaptive MR-LBM scheme “degenerating” to the reference scheme, thus $e^{0,n} \ll E^{0,n}$ for small n . On the other hand, for smooth initial data, there are many unrefined areas where either the approximation made during the stream phase (whatever the collision kernel, linear or non-linear) or the leaves collision phase (for non-linear collision kernels) generate, from the very beginning, an adaptive MR-LBM scheme which is quite different from the reference scheme. Therefore, for small n , we have either $e^{0,n} \sim E^{0,n}$ or maybe also $e^{0,n} \gg E^{0,n}$. Still, even in these cases (I and III), as long as the time grows, we are capable of largely outperforming against the reference scheme, yielding $e^{0,n} \ll E^{0,n}$ for large n .

To go further in the study, we have considered the test case III performing the collision using the reconstructed collision procedure. The result is given in Figure 2. Compared to the leaves collision (third row in Figure 1), the error $e^{0,n}$ is just divided by a factor 2 and the boundary layer close to n for $E^{0,n}/e^{0,n}$ is still present

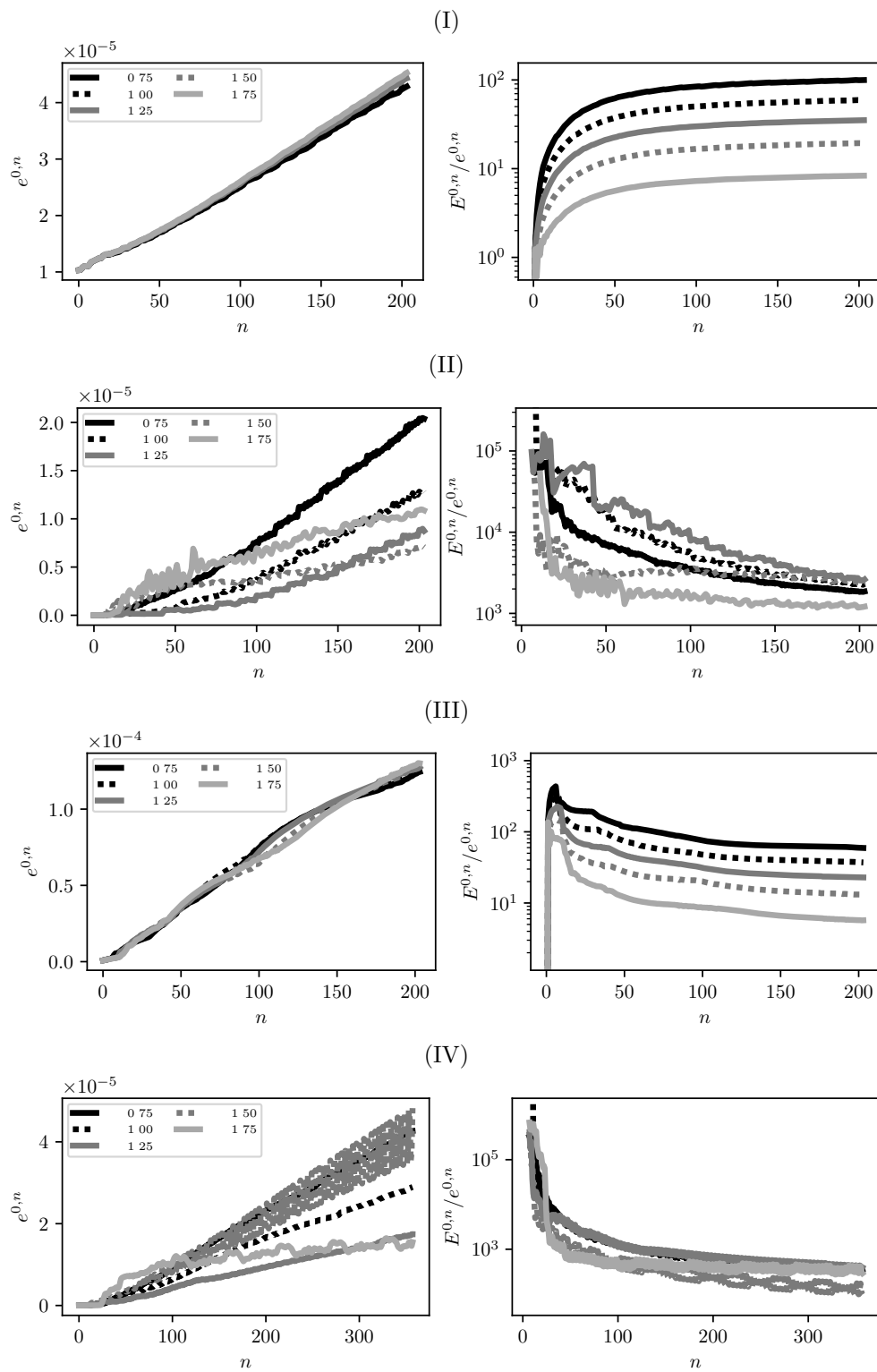


FIG. 1. Behavior of $e^{0,n}$ as function of the time (left) and the ratio $E^{0,n}/e^{0,n}$ as function of the time (right), for test (from top to bottom) I, II, III and IV.

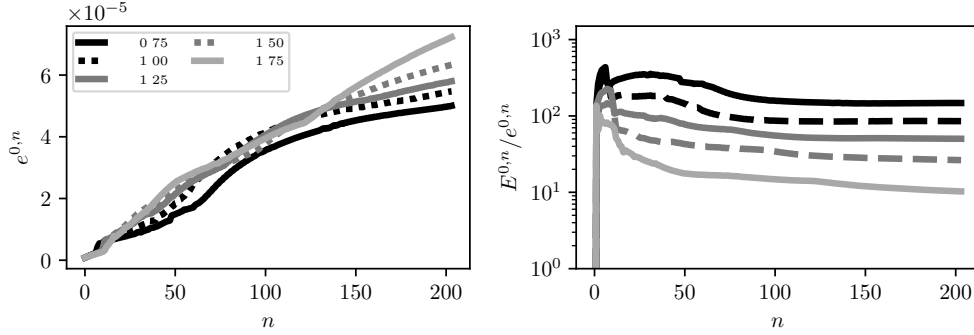


FIG. 2. Behavior of $e^{0,n}$ as function of the time (left) and the ratio $E^{0,n}/e^{0,n}$ as function of the time (right) for test III simulated using the reconstructed collision.

with values close to zero. This shows that this phenomenon is mostly inherent to the approximations made during the reconstruction employed in stream phase and in the collision phase, regardless of the fact that we use a leaves collision or a reconstructed collision. Indeed, we have exactly the same behavior once considering the leaves and the reconstructed collision for a linear collision kernel. The more the initial datum is regular, the more we can imagine this initial boundary layer tending to zero to be important.

The conclusion is that in most of the cases, both for linear and non-linear collision phases, the leaves collision is a reliable and cheaper alternative to the reconstructed collision. It has a minimal impact on the quality of the solution but results in a significant gain in terms of algorithmic efficiency.

2.1.2. Test V. In this section, we consider the Burgers equation with initial datum given by the hat-like function

$$(2.1) \quad \rho_0(x) = (1+x)\chi_{x<0}(x) + (1-x)\chi_{x\geq 0}(x).$$

This test is really interesting because we have constructed it *ad-hoc* to constitute a pathological case where the theoretical bound on the additional error by ϵ are not valid when employing the cheaper “leaves collision” *in lieu* of the “reconstructed collision”. This is due to the fact that the solution is piece-wise linear for every time – especially at initial time – and we know that the prediction operator with $\gamma = 1$ is exact on each linear branch of the solution.

Remark that the weak solution blows up at time $T^* = 1$ and we take $\bar{\mu} = 0$ in order to be sure of correctly capture the jump in the solution after this event. Moreover, the final time is taken to $T = 1.3$ to observe the blowup. The results in term of additional error $e^{0,n}$, ratio of additional and reference error $E^{0,n}/e^{0,n}$ as functions of time; trend of $e^{0,N}$ and the compression factor as function of ϵ are given in Figure 3.

Attentively looking at Figure 3, one remarks three notable facts which shall not be surprising once considering how we fabricated the solution. The first is that the temporal trend of $e^{0,n}$ changes at the blowup time $T^* = 1$. This is coherent with the fact that the solution changes its regularity from W_∞^1 to W_∞^0 (consider the effect of the details which has been fully studied in Section 1), whereas the threshold ϵ to which details are compared whilst applying \mathcal{T}_ϵ and \mathcal{H}_ϵ is kept fixed in time. Second, the ratio $E^{0,n}/e^{0,n}$ shows a time boundary layer close to $n = 0$ tending towards small

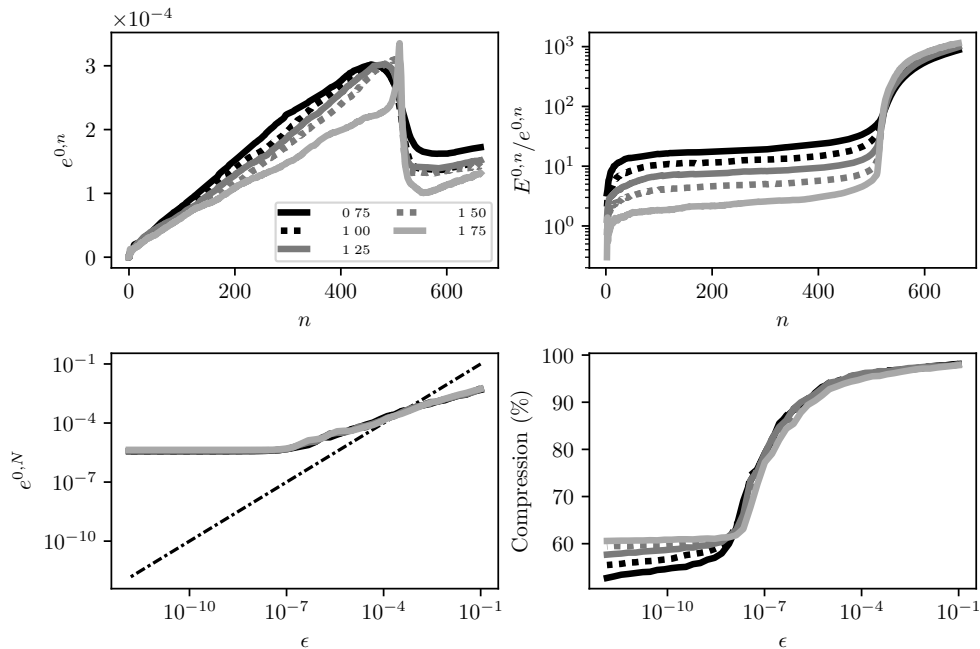


FIG. 3. Test V using the leaves collision as in the rest of the paper. On the top line, we have the additional error $e^{0,n}$ (left) and the ratio of the errors $E^{0,n}/e^{0,n}$ (right) as functions of time. On the bottom line, $e^{0,N}$ (left) and the compression factor at the final time as functions of ϵ . The dot-dashed line gives the reference $e^{0,N} = \epsilon$.

values. This means that at the very beginning of the simulation, the error of the reference scheme is comparable (or smaller) to that of the adaptive MR-LBM scheme, as we already observed for case I and III in the previous section. This fact shall be explained in a moment and we will not come to the same conclusions as in the previous section concerning the dominant causes of this phenomenon. Lastly, we observe that after an initial decrease, $e^{0,N}$ stagnates as ϵ decreases as well as the compression factor. This is in contradiction with the theoretical estimates which give $e^{0,N} \lesssim \epsilon$. However, one should not forget that we have used the “leaves collision” instead of the “reconstructed collision” and this test case has been built on purpose to obtain this.

We now provide a full explanation for these remarks, as well as an additional test. Since the initial solution is piece-wise linear, the multiresolution analysis and the grading of the tree put more and more cells close to the kinks (located at $x = -1, 0, 1$) as ϵ decreases, until reaching a point where the prediction (and thus the reconstruction) is exact and no more cell have to be added. As the reconstruction process pertains to the advection phase, from a certain ϵ and at the beginning of the simulation, the advection is exact. This is false for the collision, because of the non-linearity of the collision operator (generated by the non-linear flux $\varphi(u) = u^2/2$ pertaining to the Burgers equation). Along the sloped sides of the hat (between $[-1, 0]$ and $[0, 1]$), the collision on the leaves adds, at the very beginning of the simulation, an error which is the same for all the ϵ smaller than a certain threshold – because the initial grid is indeed the same – and which remains for the whole simulation, yielding the saturation. We have observed exactly the same saturation as ϵ decreases just compressing the mesh by multiresolution, performing the evaluation of the function

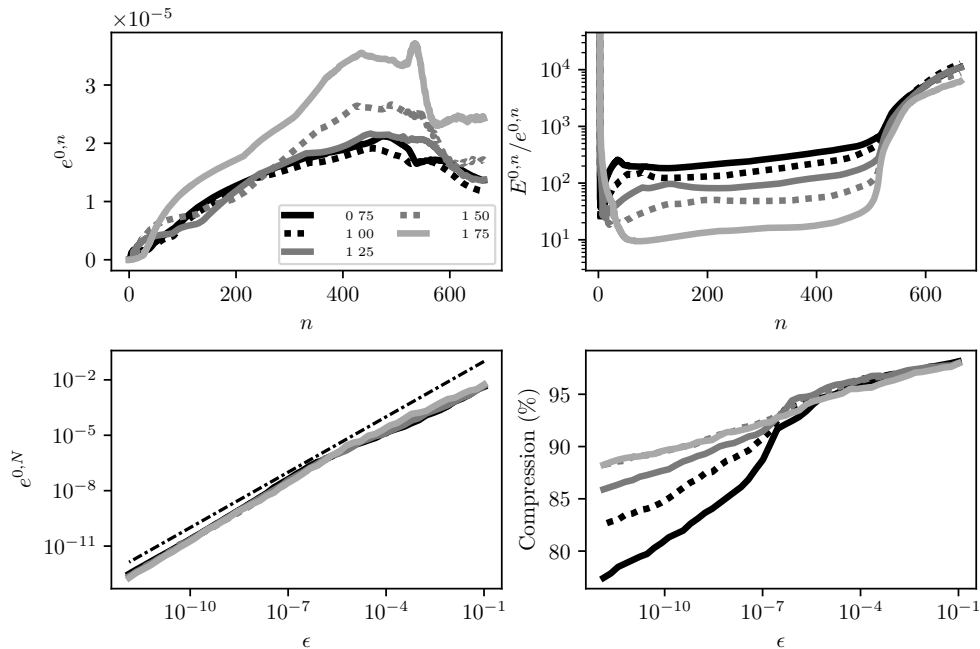


FIG. 4. Test V, using the reconstructed collision, contrarily to the rest of the paper. On the top line, we have the additional error $e^{0,n}$ (left) and the ratio of the errors $E^{0,n}/e^{0,n}$ (right) as functions of time. On the bottom line, $e^{0,N}$ (left) and the compression factor at the final time as functions of ϵ . The dot-dashed line gives the reference $e^{0,N} = \epsilon$.

$\varphi(u)$ on the leaves and measuring the error compared to the evaluation of the function $\varphi(u)$ on the full mesh at the finest level.

To corroborate our observation, we use the reconstructed collision: in this case, we recover the right estimate in ϵ , see Figure 4. This happens because the reconstruction at the finest level is exact on the slopes of the hat and thus the collision has been evaluated at the right resolution. Moreover, the behavior of the initial boundary on the plot concerning $E^{0,n}/e^{0,n}$ has been reversed, yielding large values $E^{0,n}/e^{0,n} \gg 1$ for small n . This is coherent with the other simulations with weak solutions (Figure 1), where at the beginning, the error $e^{0,n}$ is largely negligible compared to $E^{0,n}$ but is different for what happened for the regular test III, where switching from the leaves collision to the reconstructed collision did not change this initial boundary layer. Therefore, we can claim that in the setting of test V, the dominant phenomenon causing the initial boundary layer close to 0 is the leaves collision, and not a combination of stream phase and the collision phase (no matter how it is done) as for test III. Indeed, if we compare the first plot between Figure 3 and Figure 4, we notice that the tangent to the curve in the origin is way less steep in the latter case than in the former. On the other hand, for the test III in Figure 1 and 2, the tangent to $e^{0,n}$ close to $n = 0$ behaves gently both in the case of leaves collision and reconstructed collision.

Coming back to test V, in the case of leaves collision the error $e^{0,n}$ is about one order of magnitude larger than in the case of reconstructed collision. This was not the case in the previous section, where we had only a factor 2 between the errors using the leaves collision and the reconstructed collision.

To conclude, we have devised a particular case where the “reconstructed collision” is needed instead of the “leaves collision” to recover the theoretical estimates. Of course, this does not prevent us from having very interesting ratios $E^{0,n}/e^{0,n}$ far from $n = 0$ for both cases. Moreover, making the comparison between test III and V, between which the only things which changes is the initial datum, it seems clear that the reliability of the leaves collision is not so much a matter of how much the collision kernel is non-linear, but mostly a question of what is the initial datum. In the vast majority of the cases, the leaves collision is largely sufficient and does not prevent one from observing the theoretical behavior.